Solitary and cnoidal wave scattering by a submerged horizontal plate in shallow water

Masoud Hayatdavoodi, R. Cengiz Ertekin, and Benjamin D. Valentine

Citation: AIP Advances **7**, 065212 (2017); doi: 10.1063/1.4987024
View online: http://dx.doi.org/10.1063/1.4987024
View Table of Contents: http://aip.scitation.org/toc/adv/7/6
Published by the American Institute of Physics

Solitary and cnoidal wave scattering by a submerged horizontal plate in shallow water

Masoud Hayatdavoodi,[1,a] R. Cengiz Ertekin,[2] and Benjamin D. Valentine[3]
[1]*Civil Engineering Discipline, School of Science and Engineering, University of Dundee, Dundee DD1 4HN, UK*
[2]*Guest Professor, College of Shipbuilding Engineering, Harbin Engineering University, Harbin, China*
[3]*Ocean Engineering Department, Texas A&M University, Galveston, TX 77553, USA*

(Received 8 February 2017; accepted 8 June 2017; published online 23 June 2017)

Solitary and cnoidal wave transformation over a submerged, fixed, horizontal rigid plate is studied by use of the nonlinear, shallow-water Level I Green-Naghdi (GN) equations. Reflection and transmission coefficients are defined for cnoidal and solitary waves to quantify the nonlinear wave scattering. Results of the GN equations are compared with the laboratory experiments and other theoretical solutions for linear and nonlinear waves in intermediate and deep waters. The GN equations are then used to study the nonlinear wave scattering by a plate in shallow water. It is shown that in deep and intermediate depths, the wave-scattering varies nonlinearly by both the wavelength over the plate length ratio, and the submergence depth. In shallow water, however, and for long-waves, only the submergence depth appear to play a significant role on wave scattering. It is possible to define the plate submergence depth and length such that certain wave conditions are optimized above, below, or downwave of the plate for different applications. A submerged plate in shallow water can be used as a means to attenuate energy, such as in wave breakers, or used for energy focusing, and in wave energy devices. [http://dx.doi.org/10.1063/1.4987024]

I. INTRODUCTION

This study is concerned with the propagation of nonlinear water waves of solitary and cnoidal types over a fully submerged, horizontal, flat plate in shallow water. The presence of the submerged fixed plate in the flow field results in the separation of the fluid domain above and below the structure. Above the plate, the wave height initially increases due to the sudden reduction in water depth, and the wave undergoes significant deformation. Below the plate, the vertical particle velocity is zero and the flow is uniform and oscillatory. Consequently, part of the wave energy reflects back upwave of the plate, and the transmitted energy downwave of the plate may be scattered. Hence, the transmitted wave height will be smaller than the incident wave.

A pile-supported or moored horizontal plate may be utilized as a breakwater to mitigate severity of waves approaching shoreline. A submerged breakwater can preserve some of the natural water circulation downwave of the object, it does not create visual obstruction, it is simple and relatively inexpensive to build and maintain (when compared with the mound structures), and hence it is an attractive alternative for protection of coastlines. Laboratory experiments of Brossard et al. (2009) show that a submerged plate is more efficient in scattering the wave energy than a submerged step of the same length. A submerged plate can be used for protection of marine aquaculture regions, or be used directly for oyster farming, for example. A submerged plate can also act as a major component of wave energy devices, see *e.g.* Carter and Ertekin (2014). A combination of breakwater-energy

[a]Corresponding Author; Electronic mail: mhayatdavoodi@dundee.ac.uk

converter system is also considered, see Graw (1993). Moreover, submerged plates are used for wave focusing and wave amplification in wave-energy converters, see *e.g.* Stamnes et al. (1983); Martin and Farina (1997); Newman (2015); Duffett et al. (2016). An oscillating submerged plate may be used as the core component of a wave energy device, see Hayatdavoodi et al. (2016, 2017), or as a heaving plate in controlling the motion of offshore platforms, see Martin and Farina (1997) and Farina (2010), among others.

Here, we are specifically concerned with the unsteady solution of the problem of nonlinear, regular waves propagating over a two-dimensional, solid, submerged, horizontal plate. The plate is considered thin, assuming the thickness is much smaller than the length or width of the structure and the water depth. The seafloor beneath the submerged plate is assumed flat, although this is not always necessary.

When applying the linear water wave theory to wave interaction with a fixed, horizontal, flat plate, it is possible to form, and analytically solve, a closed-form boundary-value problem for the flow field. This approach is used by Stoker (1958) and Siew and Hurley (1977) to study the problem of propagation of small-amplitude waves over a submerged plate in shallow water, where wavelength (λ) is assumed to be much larger than water depth $\lambda \gg h$, *i.e.* long waves. Moreover, to find a closed form of the equations, Siew and Hurley (1977) assumed that the plate length (L_p) is much larger than the water depth, $L_p \gg h$. The domain is then divided into separate regions, subject to linear boundary conditions, and a matched asymptotic expansion method is used to obtain the solution. Similar approach is used by McIver (1985); Liu and Iskandarani (1991); Kojima et al. (1994) for deep-water waves, who solved the system of equations by use of an eigenfunction expansion method. Liu (1984), and more recently, Lo and Liu (2014), used this approach to study the diffraction of solitary waves by a submerged plate.

It is not, however, always possible to solve the linear boundary-value problem analytically, for example for the problem of interaction of linear waves with structures of arbitrary shapes, located at or below the surface. In approaching such problems, and within the usual assumptions of inviscid fluid and incompressible and irrotational flow, the flow field is defined by the use of a velocity potential.

The boundary-value problem is then solved either numerically, *e.g.* by Finite Element Method (FEM), or by semi-analytical methods such as the Green Function Method. The Boundary Element Method is used by Liu and Abbaspour (1982) to study the interaction of linear waves with a submerged plate, followed by Parsons and Martin (1992); Zhang and Williams (1996); Farina and Martin (1998); Hsu and Wu (1998); Lalli et al. (2008), among others, and more recently by Ning et al. (2015). Heins (1948); Greene and Heins (1953); Burke (1964) used the Wiener-Hopf technique to solve the boundary-value problem of scattering of small-amplitude waves by a submerged plate in deep water. A finite-element method is used by Patarapanich and Cheong (1989) to solve the linear wave diffraction problem for interaction of regular and random waves with a submerged, horizontal thin plate.

For most of the interesting wave-structure interaction problems, however, the linear free surface assumption breaks down, *i.e.*, waves are nonlinear. Classically, the problem of propagation of nonlinear shallow-water waves is studied by use of a perturbation approach, assuming the flow can be governed by Laplace's equation, however, subject to nonlinear free-surface boundary conditions. The nonlinear boundary condition is then approximated by use of a perturbation expansion. A small perturbation parameter is obtained by making *a priori* assumptions about the flow field. The unknown velocity potential and surface elevation are then expanded around the linear solution by use of the small perturbation parameter. The classical Boussinesq-type equations (see Boussinesq (1871) and Korteweg and De Vries (1895)), follow this approach, see *e.g.* Wu (1981); Wu and Wu (1982); Kim and Bai (2004) for further discussion and some application of these equations. Further information about nonlinear shallow-water waves can be found in, for example, a recent review by Ertekin and Rodenbusch (2016).

The Boussinesq-type equations are used in a number of nonlinear shallow-water wave problems, for example in nonlinear wave propagation over a sloping beach (see Nwogu (1993); Wei et al. (1995); Madsen and Schäffer (1998); Gobbi et al. (2000)) and shallow-water wave propagation over a submerged bar (Beji and Battjes (1994); Ohyama et al. (1995)). To the authors' knowledge, the problem of wave interaction with a submerged plate has not been studied by these perturbation-based, nonlinear, shallow-water wave equations.

In recent years, and with the progress in computational methods and resources, the problem of interaction of nonlinear waves with submerged obstacles has been studied using the computational fluid dynamics (CFD) approach. Assumptions of inviscid fluid and irrotational flow are released and the governing equations are changed to the Navier-Stokes (N-S) equations. Such methods are use by, *e.g.* Huang and Dong (1999) for wave propagation over a submerged dike, and by Carter et al. (2006); Lo and Liu (2014); Hayatdavoodi et al. (2015) for wave interaction with a submerged plate.

Yet another alternative is that employed by Green and Naghdi (1976b,a), who constructed a nonlinear wave theory on directed fluid sheets. Green and Naghdi obtained a fairly general theory that has its roots in the theory of plates and shells (Green et al. (1974)). The resultant fluid flow governing equations, namely the Green-Naghdi theory of water waves (GN hereafter), is applicable to propagation of nonlinear waves in an incompressible medium. The theory considers a three-dimensional body of the fluid, known as the fluid sheet, and satisfies exactly the boundary conditions on the top and bottom surfaces (the free surface and seafloor boundaries, respectively) of the fluid sheet, and postulates the integrated conservation laws. In the general form of the theory, incompressibility is the only assumption made about the medium. The fluid does not need to be inviscid and it is not necessary for the flow to be irrotational, although the equations can also be governed by assuming an irrotational flow, see Kim and Ertekin (2000); Kim et al. (2001, 2003); Ertekin et al. (2014). The only assumption made about the kinematics of the flow is the distribution of the vertical velocity over the fluid sheet. The theory is classified based on the order of the polynomials used to describe this distribution. In the Level I GN equations, for example, a linear distribution of the vertical velocity and constant distribution of horizontal velocity are considered, see Section II for the details. Each increasing Level corresponds to an increasing number of governing equations, and in principle to increasing level of accuracy. See *e.g.* Webster and Shields (1991); Zhao et al. (2014a, 2015) for discussion and application of higher-level GN equations. Further information about the GN theory can be found in, *e.g.*, Ertekin (1984); Shields and Webster (1988); Demirbilek and Webster (1992); Webster and Wehausen (1995); Demirbilek and Webster (1999). In this paper, we will use the Level I GN theory to study the problem of nonlinear wave propagation over a submerged horizontal plate in shallow water.

In recent years, and with the development of computational tools, a number of particle-based methods have been used to study wave transformation and interaction with submerged obstacles, see *e.g.* Wei and Dalrymple (2016); Sampath et al. (2016). Further details on different theoretical approaches used to study the problem of wave interaction with a submerged plate can be found in a recent review by Hayatdavoodi and Ertekin (2016).

Laboratory experiments on wave interaction with submerged plates in deep and intermediate water are conducted by Dick and Brebner (1968); Dattatri et al. (1977); Neelamani and Reddy (1992); Brossard and Chagdali (2001); Liu et al. (2009); and Brossard et al. (2009), among others. Experiments on solitary and cnoidal wave scattering by a submerged plate are conducted by Lo and Liu (2014); Seiffert et al. (2014); Hayatdavoodi et al. (2015), with emphasis on the wave-induced forces on the object.

Here, attention is confined to the interaction of regular, non-breaking water waves with a two-dimensional, impermeable, rigid, submerged plate that is fixed at all times. A number of other studies have focused on the interaction of water waves with submerged plates with different characteristics. See, *e.g.*, Yu and Chwang (1994) for effect of plate porosity on the flow field, Usha and Gayathri (2005); Cho et al. (2013) for effect of multiple submerged horizontal plates, and Hassan et al. (2009); Williams and Meylan (2012) for wave interaction with an elastic plate. The Level I GN equations are used by Hayatdavoodi and Ertekin (2017) to study the interaction of periodic waves with a submerged elastic plate. The three-dimensional wave scattering by submerged disks is studied by, *e.g.*, Yu and Chwang (1993).

Most of the applications of submerged plates in wave control or energy extraction is in shallow waters, and in the presence of nonlinear waves. Most of the works in literature, however, are concerned with deep to intermediate water conditions, and use theoretical approaches that are not suitable for propagation of nonlinear long waves. Nonlinear shallow-water waves are fundamentally different from linear waves, or nonlinear deep-water waves. Consequently, the wave scattering by a submerged plate in shallow water posses some specific characteristics due to nonlinear wave conditions.

Our objectives in this work are to (i) formulate the problem of nonlinear wave scattering by a submerged plate by use of the Level I GN equations, (ii) study interaction of nonlinear waves of cnoidal and solitary types with a submerged plate in shallow water, (iii) define and asses the use of reflection and transmission coefficients in analyzing results of the fundamentally nonlinear theory, and (iv) study solitary wave scattering by a submerged plate. Results of the GN equations are compared with the existing laboratory measurements and other theoretical solutions (in deep to intermediate depths), and the wave scattering is analyzed by performing a parametric study.

The Level I Green-Naghdi theory, and its application to the problem of propagation of long waves over a submerged plate are discussed in Section II. The wave scattering by the submerged plate in intermediate and deep waters is studied by defining reflection and transmission coefficients, and the GN results are compared with the laboratory experiments and other existing theoretical solutions. The procedure in defining the coefficients is given in Section III, followed by a comparison and discussion of the GN results in Section IV. The paper is closed by the concluding remarks.

II. THE LEVEL I GREEN-NAGHDI EQUATIONS

The Level I GN equations are used here in their two-dimensional form. A right-handed Cartesian coordinate system, with x_1 pointing to the right and x_2 directed against gravity is considered, where the origin of the coordinate systems is on the still-water level (SWL). Here, SWL refers to the undisturbed water level in the absence of waves. The fluid is inviscid and the flow is incompressible, but irrotationality is not required. In the Level I GN equations, it is assumed that the vertical velocity, $u_2(x_1, x_2, t)$, varies linearly along the water column. This assumption, along with the incompressibility condition, results in constant horizontal velocity in the vertical direction, *i.e.*, $u_1(x_1, x_2, t) = u_1(x_1, t)$; a condition that is mostly applicable to propagation of long waves. Here, t stands for time. The free surface, $\eta(x_1, t)$, is measured from the SWL. The Level I equations as used here are given by (Ertekin (1984)):

$$\eta_{,t} + \{(h + \eta - \alpha)u_1\}_{,x_1} = \alpha_{,t}, \tag{1a}$$

$$\dot{u}_1 + g\eta_{,x_1} + \frac{\hat{p}_{,x_1}}{\rho} = -\frac{1}{6}\{[2\eta + \alpha]_{,x_1}\ddot{\alpha} + [4\eta - \alpha]_{,x_1}\ddot{\eta} + (h + \eta - \alpha)[\ddot{\alpha} + 2\ddot{\eta}]_{,x_1}\}, \tag{1b}$$

$$u_2(x_1, x_2, t) = \dot{\alpha} + \frac{(x_2 + h - \alpha)}{(\eta + h - \alpha)}(\dot{\eta} - \dot{\alpha}), \tag{1c}$$

$$P(x_1, t) = \left(\frac{\rho}{6}\right)(h + \eta - \alpha)^2(\ddot{\alpha} + 2\ddot{\eta} + 3g) + \hat{p}(h + \eta - \alpha), \tag{1d}$$

$$\bar{p}(x_1, t) = \left(\frac{\rho}{2}\right)(h + \eta - \alpha)(\ddot{\alpha} + \ddot{\eta} + 2g) + \hat{p}, \tag{1e}$$

where $\alpha(x_1, t)$ is the vertical location of the bottom of the fluid sheet, h is the water depth, ρ is the mass density of the fluid, g is the gravitational acceleration. The Latin subscripts with comma are partial differentiation with respect to the indicated variables, and superposed dot is the two-dimensional material time derivative. $u_2(x_1, x_2, t)$ is the vertical component of particle velocity. P is the integrated (over the water column) pressure, $\bar{p}$ is the pressure on the bottom curve (α) of the fluid sheet, and $\hat{p}(x_1, t)$ is the pressure on the top curve of the fluid sheet. Hayatdavoodi (2013) and Hayatdavoodi and Ertekin (2015b) applied the Level I GN equations to the problem of propagation of an inviscid and incompressible fluid over a fully submerged, horizontal flat plate in shallow water, with emphasis on determining the wave-induced loads on the plate. A comparative study of nonlinear wave interaction with a submerged plate by use of the GN equations and a CFD approach is given by Ertekin and Hayatdavoodi (2015).

A. The domain equations

In this approach, the plate is thin (zero thickness in theory) and the continuum domain is separated into four regions, namely Region RI upwave of the plate, Region RII above the plate, Region RIII beneath the plate, and Region RIV downwave. Each of the regions is subject to specific boundary conditions. The leading and trailing edges of the plate are fixed at $x_1 = X_L$ and $x_1 = X_T$, respectively. At the discontinuity curves, namely the leading and trailing edges of the plate, certain conditions

are enforced to ensure satisfaction of the conservation laws and a continuous solution in the entire domain. A schematic of the fluid domain is shown in Fig. 1.

In Regions RI and RIV, upwave and downwave of the plate, we are concerned with the propagation of nonlinear waves over a flat and stationary seafloor ($\alpha = 0$). The top surface, η, is free and subject to the atmospheric pressure taken as $\hat{p} = 0$, without loss in generality. Hence, in RI and RIV regions, the GN equations (1), are given as

$$\eta_{,t} + \{(h_I + \eta)u_1\}_{,x_1} = 0, \tag{2a}$$

$$\dot{u}_1 + g\eta_{,x_1} = -\frac{1}{3}\{(2\eta_{,x_1}\ddot{\eta}) + (h_I + \eta)\,\ddot{\eta}_{,x_1}\}, \tag{2b}$$

$$u_2 = \frac{(x_2 + h_I)}{(\eta + h_I)}\dot{\eta}, \tag{2c}$$

$$P = \left(\frac{\rho}{6}\right)(h_I + \eta)^2\,(2\ddot{\eta} + 3g)\,, \tag{2d}$$

$$\bar{p} = \left(\frac{\rho}{2}\right)(h_I + \eta)\,(\ddot{\eta} + 2g)\,. \tag{2e}$$

where h_I is the constant water depth in RI and RIV. The explicit unknowns in RI and RIV regions are the surface elevation (η) and horizontal velocity (u_1).

Region RII, above the plate, is subject to atmospheric pressure on the top surface, $\hat{p} = 0$, and constant water depth above the plate $h_{II} = d$. In this study, the plate is rigid, horizontal and fixed at all times. Hence the bottom surface of the fluid sheet, *i.e.* the plate, is stationary: $\alpha(x_1, t) = 0$. The GN equations (1), for this region are given as

$$\eta_{,t} + \{(d + \eta)u_1\}_{,x_1} = 0, \tag{3a}$$

$$\dot{u}_1 + g\eta_{,x_1} = -\frac{1}{3}\left\{(2\eta_{,x_1}\ddot{\eta}) + (d + \eta)\,\ddot{\eta}_{,x_1}\right\}, \tag{3b}$$

$$u_2 = \frac{(x_2 + d)}{(\eta + d)}\,\dot{\eta}, \tag{3c}$$

$$P = \left(\frac{\rho}{6}\right)(d + \eta)^2\,(2\ddot{\eta} + 3g)\,, \tag{3d}$$

$$\bar{p} = \left(\frac{\rho}{2}\right)(d + \eta)\,(\ddot{\eta} + 2g)\,. \tag{3e}$$

Similar to RI and RIV regions, the explicit unknowns in RII are the surface elevation (η) and horizontal velocity (u_1).

In Region RIII, below the plate, the top surface is the fixed plate. The water depth is constant $h = h_{III}$, and surface elevation is zero $\eta = 0$. We assume horizontal and stationary seafloor $\alpha(x_1, t) = 0$.

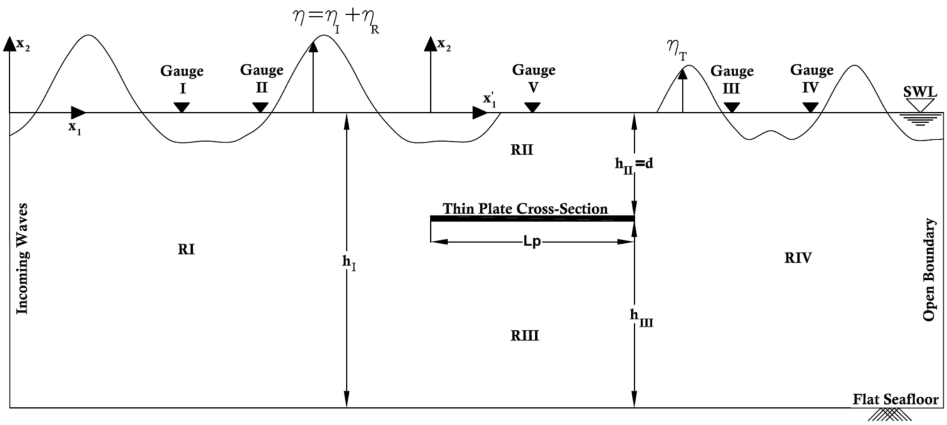

FIG. 1. Schematic of the theoretical wave tank of nonlinear wave propagation over a submerged plate, showing the four regions and relative location of the wave gauges discussed within the text.

The $\eta = 0$ condition in this region ($X_L < x_1 < X_T$ & $-h_I \le x_2 \le -d$) simplifies the GN equations significantly, and the flow governing equations (1), reduce to

$$u_1(x_1,t) = u_1(t) = -\frac{1}{\rho}\int \hat{p}_{,x_1}(t')\,dt', \tag{4a}$$

$$\hat{p}(x_1',t) = -\int (\rho u_{1,t})\,dx_1' = -\rho u_{,t} x_1' + C(t), \tag{4b}$$

$$u_2(x_1,x_2,t) = 0, \tag{4c}$$

$$P = \frac{1}{2}\left(\rho g h_{III}^2\right) + \hat{p}h_{III}, \tag{4d}$$

$$\bar{p} = (\rho g h_{III}) + \hat{p}, \tag{4e}$$

where $C(t)$ is the integration constant and x_1' is measured from an arbitrary reference point in RIII, at which $\hat{p}(0,t) = C(t)$. Equation (4c), the zero vertical velocity under the plate, is obtained by substituting $\eta = 0$ condition of RIII into the equation of the vertical velocity, Eq. (1c). Equation (4a), direct result of substituting $\eta = 0$ into the conservation of mass equation for an incompressible fluid flow (1a), shows a uniform flow field under the plate at each time step, similar to the Coutte flow between two parallel walls. The driving force in RIII is the pressure differential between the two ends of the region. Equation (4b) presents a linear distribution of top pressure underneath the plate. The explicit unknowns in RIII are the top pressure ($\hat{p}$) and the horizontal velocity (u_1).

In the limit of a "long" plate, $x_1' \to \infty$, Eq. (4b) results in $\hat{p}(x_1',t) \to \infty$, *i.e.* plate bottom pressure at the edges will be unbounded. This condition is not physical and hence, Eq. (4b) is not applicable to "long" plates. To obtain a physical solution for $\hat{p}$ at this limit, and recalling from (4b) that $\hat{p}$ varies linearly in Region III at all times, we assume $\hat{p}$ in Region III varies linearly between the leading and trailing edges of the plate, *i.e.*

$$\hat{p}(x_1',t) = \left(\frac{\hat{p}(X_T,t) - \hat{p}(X_L,t)}{X_T - X_L}\right)x_1' + \hat{p}(X_L,t), \quad X_L \le x_1' \le X_T, \tag{5}$$

where $\hat{p}(X_L,t)$ and $\hat{p}(X_T,t)$ are the plate bottom pressures at the leading and trailing edges, respectively. In the limit of $x_1' \to 0$ of a "short" plate, Eqs. (5) and Eq. (4b) are identical.

The fluid motion inside Region III is determined by integrating Eq. (4a) with respect to t:

$$u_1(x_1,t) = u_1(t) = -\frac{1}{\rho}\int \hat{p}_{,x_1}(t')\,dt', \quad X_L < x_1 < X_T, \tag{6}$$

where $\hat{p}_{x_1}$ is calculated by differentiating Eq. (5).

The GN equations of the four regions satisfy the free surface and bottom boundary conditions exactly. To obtain a continuous solution in the entire domain, jump and matching conditions are enforced at the discontinuity curves where the regions meet.

B. The jump and matching conditions

At the leading and trailing edges of the plate, where three different regions meet, $x_1 = X_L$ and $x_1 = X_T$, functions $\eta(x_1,t)$, $u_1(x_1,t)$, $\bar{p}(x_1,t)$ and $\hat{p}(x_1,t)$ and their spatial derivatives are no longer necessarily continuous. We recall from the Appendix section of Hayatdavoodi and Ertekin (2015b), the appropriate form of the jump conditions demanded by the theory to match the solution on either side of the discontinuity curves. The jump conditions are given by

$$[[\rho\varphi u_1]]_{\bar{X}} = 0, \tag{7a}$$

$$[[\rho\varphi u_1^2 + P]]_{\bar{X}} = F_1, \tag{7b}$$

$$[[\frac{1}{2}\rho\varphi u_1 w]]_{\bar{X}} = F_3, \tag{7c}$$

$$[[\frac{1}{12}\rho\varphi u_1 w]]_{\bar{X}} = L_3, \tag{7d}$$

where $\varphi = \eta + h$ is the thickness of the fluid sheet, $w = \dot{\phi}$, and the subscript $\bar{X} = X_L$ and $\bar{X} = X_T$ when writing the jump conditions for the discontinuity curve at the leading edge and trailing edge, respectively, and

$$F_1 = \lim_{\delta \to 0} \int_{\bar{X}-\delta}^{\bar{X}+\delta} \left(\hat{p}\varphi_{,x_1} - \bar{p}\alpha_{,x_1}\right) \mathbf{e_1}\, dx_1, \tag{8a}$$

$$F_3 = \lim_{\delta \to 0} \int_{\bar{X}-\delta}^{\bar{X}+\delta} \left(\bar{p} - \hat{p}\right) \mathbf{e_3}\, dx_1, \tag{8b}$$

$$L_3 = \lim_{\delta \to 0} \int_{\bar{X}-\delta}^{\bar{X}+\delta} -\frac{1}{2}\left(\bar{p} + \hat{p}\right) \mathbf{e_3}\, dx_1. \tag{8c}$$

In Eqs. (7), the notation $[[f]]_{\bar{X}}$, where f is any function, stands for the jump in f across the discontinuity curves, *i.e.*,

$$[[f]]_{\bar{X}} = f^+_{\bar{X}} - f^-_{\bar{X}}, \text{ where } f^+_{\bar{X}} = \lim_{x_1 \to \bar{X}^+} f \text{ and } f^-_{\bar{X}} = \lim_{x_1 \to \bar{X}^-} f. \tag{9}$$

In Eqs. (7), F_1, F_3 and L_3, arise from non-vanishing integrable singularities of $\hat{p}$, $\bar{p}$ and $\varphi_{,x_1}$ on the discontinuity curves, and they result in the balance of the jump in the horizontal component of linear momentum, the jump in the vertical component of linear momentum and the jump associated with the moment of momentum (director momentum), respectively. Equation (7a) ensures the mass conservation across the discontinuity curve.

In addition to the jump conditions, two matching conditions are enforced at the discontinuity curves, motivated by the physics of the fluid around the plate. First, we require that the top surface remain continuous across the discontinuity curves, given as

$$[[\eta]]_{\bar{X}} = 0, \quad \text{at} \quad x_2 = \eta \quad \text{and} \quad \bar{X} = X_L \quad \& \quad \bar{X} = X_T. \tag{10}$$

Recall that $\eta(x_1, t) = 0$ in RIII. From $\varphi = \eta + h$ and for a constant water depth ($h = h_I$), condition (10) reads

$$[[\varphi]]_{\bar{X}} = 0, \quad \text{at} \quad \bar{X} = X_L \quad \& \quad \bar{X} = X_T, \tag{11}$$

or

$$h_I = d + h_{III}, \quad \text{at} \quad \bar{X} = X_L \quad \& \quad \bar{X} = X_T, \tag{12}$$

i.e., the plate is thin (as assumed in this model).

We also require continuous pressure on the seafloor at the discontinuity curves, X_L and X_T, such that

$$[[\bar{p}]]_{\bar{X}} = 0 \quad \text{at} \quad x_2 = -h_I \quad \text{and} \quad \bar{X} = X_L \quad \& \quad \bar{X} = X_T. \tag{13}$$

Condition (13) is written at $x_1 = X_L$ as

$$\bar{p}_{III} - \bar{p}_I = 0, \quad \text{at} \quad x_1 = X_L, \tag{14}$$

where $\bar{p}_I$ and $\bar{p}_{III}$ are the bottom pressure of RI and RIII, receptively. Substituting Eqs. (2e) and (4e) into Eq. (14), and adding the force on the fluid due to the jump conditions (7), we have

$$(\rho g h_{III}) + \left(\hat{p}\left(X_L, t\right) - \frac{F_{3X_L} + L_{3X_L}}{h_I}\right) - \left(\frac{\rho}{2}\right)\left(h_I + \eta\left(X_L, t\right)\right)\left(\ddot{\eta}\left(X_L, t\right) + 2g\right) = 0, \tag{15}$$

or

$$\hat{p}\left(X_L, t\right) = \left(\frac{\rho}{2}\right)\left(h_I + \eta\left(X_L, t\right)\right)\left(\ddot{\eta}\left(X_L, t\right) + 2g\right) - \left(\rho g h_{III}\right) + \left(\frac{F_{3X_L} + L_{3X_L}}{h_I}\right), \tag{16}$$

where, F_{3X_L} and L_{3X_L} are the resultant forces at the leading edge of the plate due to the jump condition (7). Similarly, $\hat{p}\left(X_T, t\right)$ is written as

$$\hat{p}\left(X_T, t\right) = \left(\frac{\rho}{2}\right)\left(h_I + \eta\left(X_T, t\right)\right)\left(\ddot{\eta}\left(X_T, t\right) + 2g\right) - \left(\rho g h_{III}\right) + \left(\frac{F_{3X_T} + L_{3X_T}}{h_I}\right), \tag{17}$$

where, F_{3X_T} and L_{3X_T} are the forces on the plate due to the jump conditions at the trailing edge of the plate, given in Eq. (7c).

Note that it is possible to obtain a solution for the problem by specifying a constitutive equation for the force on the fluid sheet at the leading and trailing edges under any physical condition. This

would require *a priori* knowledge of the forces due to the jumps. Here, however, we avoid the necessity of explicitly specifying constitutive equations. The above matching conditions result in system of equations that satisfy the governing equations, boundary conditions and the jump conditions of the theory, exactly.

In this study, the function η is single-valued, and hence all cases considered are concerned with non-breaking waves. In the absence of use of any scaling parameter in the derivation of the GN equations, in any level of the theory, limitations of the applicability of the theory to a given problem is set by the numerical schemes used to solve the equations.

Hereafter, we use h for the constant water depth upwave and downwave of the plate, and d for the water depth above the plate, also referred to as the submergence depth of the thin plate. λ and H refer to the incident (un-scattered) wavelength and wave height, respectively, and L_p is the plate length, in the wave propagation direction.

C. The wavemaker

On the left side of RI upwave, a numerical wavemaker capable of generating solitary and cnoidal waves is installed. Solitary solution of the GN equations is given by Green et al. (1974)

$$\eta(\bar{x},0) = A\, sech^2\left(\epsilon\bar{x}\right), \tag{18a}$$

$$u_1(\bar{x},0) = \sqrt{g(A+h)}\frac{A\, sech^2\left(\epsilon\bar{x}\right)}{h + A\, sech^2\left(\epsilon\bar{x}\right)}, \tag{18b}$$

where

$$\epsilon = \sqrt{\frac{3A}{4h^2(A+h)}}, \tag{19}$$

and $\bar{x} = x_1 - x_0 - Ut$, where x_0 is the location of the center of the solitary wave at time $t = 0$ and A is the solitary wave amplitude. $U = \sqrt{g\left(A+h\right)}$ is the propagation speed of the solitary wave over a flat seafloor. The vertical component of particle velocity, $u_2(\bar{x}, x_2, 0)$, under the GN solitary wave is given by Hayatdavoodi and Ertekin (2015c)

$$u_2(\bar{x},x_2,0) = \frac{x_2}{h + A\, sech^2\left(\epsilon\bar{x}\right)}\left(2A\, sech^2\left(\epsilon\bar{x}\right)\tanh\left(\epsilon\bar{x}\right)\right)\left(\sqrt{g(A+h)} - u_1(\bar{x},0)\right). \tag{20}$$

The cnoidal solution of the Level I GN equations can only be obtained in a semi-closed form when the water depth is constant in the vicinity of the wavemaker. Let us define a moving coordinate in the form of $\hat{x} = x_1 - ct$, where c is the wave phase speed, *i.e.*, the constant speed of the right-moving coordinate. Note that the right-moving coordinate is only used at the location of the wavemaker. A periodic solution of the Level I GN equations is given in the moving coordinate as (see Sun (1991) and Ertekin and Becker (1998))

$$\bar{\eta}(\hat{x}) = \eta_2 + \bar{H}\mathbf{Cn}^2(\xi,k), \quad \bar{u}(\hat{x}) = \frac{c\bar{\eta}(\hat{x})}{1+\bar{\eta}(\hat{x})}, \tag{21}$$

where the constant phase speed c, is given by

$$c = \sqrt{(1+\eta_1)(1+\eta_2)(1+\eta_3)}, \tag{22}$$

and

$$\eta_1 = -\frac{\bar{H}}{k^2}\frac{E(k)}{K(k)}, \quad \eta_2 = \frac{\bar{H}}{k^2}\left(1 - k^2 - \frac{E(k)}{K(k)}\right), \quad \eta_3 = \frac{\bar{H}}{k^2}\left(1 - \frac{E(k)}{K(k)}\right), \tag{23}$$

where

$$k^2 = \frac{\bar{H}}{\eta_3 - \eta_1}, \ \xi = \frac{2K(k)}{L}\hat{x}, \ L = kK(k)\sqrt{\frac{16}{3\bar{H}}(1+\eta_1)(1+\eta_2)(1+\eta_3)}, \tag{24}$$

and $\mathbf{Cn}(\xi,k)$ is the Jacobian elliptic cosine function with an argument ξ and modulus k, and $K(k)$ and $E(k)$ are the complete elliptic integrals of the first and second kind, respectively. We note that the physical variables are given in dimensionless form by selecting (ρ, g, h) as a dimensionally independent set:

$$\bar{\eta} = \frac{\eta}{h}, \ \bar{u} = \frac{u}{\sqrt{gh}}, \ \bar{H} = \frac{H}{h}, \ \bar{\lambda} = \frac{\lambda}{h}. \tag{25}$$

The wavelength $\bar{\lambda}$ is calculated using the below dispersion relation:

$$\bar{\lambda} = kK(k)c\sqrt{\frac{16}{3\bar{H}}}. \tag{26}$$

An iterative approach is used to solve Eqs. (21) and (26). The wavemaker motion is then described by

$$\eta(0,t) = \eta_0(t)\,, \quad u(0,t) = u_0(t), \tag{27}$$

where $t \geq 0$, and η_0 and u_0 are specified by Eq. (21). For the cases studied in this work, we define the length of the upwave region, RI, and the computational time such that the reflected waves from the plate do not interfere with the wavemake. For further examples of waves generated by the GN theory see, *e.g.*, Demirbilek and Webster (1992), Ertekin et al. (2014) and Zhao et al. (2014b).

D. The open boundary

On the right hand side of RIV, downwave from the plate, an open boundary is set up to minimise the wave reflection to the tank. Previous works of Wu and Wu (1982) and Ertekin (1984) have shown that a relatively simple open-boundary condition is sufficient in preventing significant reflection from the boundary. We use the Orlanski's condition at this boundary, $\Omega_{,t} + c\Omega_{,x_1} = 0$, where Ω may be η or u_1, and c is the constant, linear shallow-water phase speed $c = \pm\sqrt{gh}$.

E. The numerical solution

The governing equations in the four regions, along with the jump and matching conditions, are solved simultaneously for the unknowns. The system of equations is solved numerically by the central-difference method, second-order in space, and with the Modified-Euler Method for time marching. Further details about the numerical solution of the Level I GN equations can be found in Hayatdavoodi and Ertekin (2015c).

Note that in this model, the plate is thin. Computational results of Lalli et al. (2008) on wave interaction with a submerged breakwater, obtained by use of the boundary element method, show that the thickness of the plate does not play significant role on wave scattering. They quantitatively showed that the reflected and transmitted waves do not alter as the plate thickness change for the $t_p \ll h$ condition. Similar conclusion is made by Liu et al. (2009) for wave scattering by a submerged plate through laboratory measurements, and through computations and measurement of wave-induced loads on submerged plates and boxes by Hayatdavoodi et al. (2014) and Hayatdavoodi and Ertekin (2015a), respectively.

We note that in this study, the fluid is inviscid. Presence of the submerged plate in a viscous fluid may result in formation of eddies and vortices at the leading and trailing edges of the plate due to the shear stresses near the boundary. See Poupardin et al. (2012) and Pinon et al. (2016) for laboratory experiments and computations on kinematics of wave-induced vortices around a submerged plate. The vortices, in return, may cause some wave deformations. The energy dissipation due to the formation of the vortices is relatively small, particularly when the plate is submerged at deeper depths. Moreover, laboratory experiments conducted by Brossard et al. (2009) show that the oscillations generated by the vortices are negligible. Such effects, associated with viscous stresses, are not considered in the inviscid model used here.

III. REFLECTION AND TRANSMISSION COEFFICIENTS

In studying wave scattering by a submerged plate, a classical approach has been to define reflection and transmission coefficients and associate the energy distribution to these coefficients. Change of the water depth due to the slope on the seafloor or presence of a submerged obstacle can lead to generation of some modes of oscillation which occur at discrete frequencies. The oscillations are confined to some localized regions near the variable slope or the submerged obstacle. Within the linear theory, and to obtain a definition for the reflection and transmission coefficients, it is necessary to distinguish these localized oscillations from the progressive wave components.

The topic of localized periodic waves was perhaps first discussed in the pioneering work of Stokes (1846) on the propagation of water waves over uniformly sloping beaches. Stokes (1846) describes the generation of a wave that can travel unchanged in the direction of the shoreline (perpendicular to the incident wave direction), which decays almost exponentially to zero in the upwave direction.

Existence of such oscillating modes above submerged obstacles were discussed later by Ursell (1951). Such localized oscillations are often referred to as edge wave in applications of wave propagation over sloping beaches, and trapped phase-locked or bound modes in the context of wave scattering due to submerged obstacles. A distinguishing characteristic of a trapped wave is that it is confined to or trapped by the boundary, in this case the submerged plate, even though the fluid region is unbounded. Many have shown that trapped-modes exist in a wide class of problems including that of wave interaction with a submerged, long two-dimensional obstacle (Newman (1965)), submerged elliptical torus (McIver and Porter (2002)), submerged cylinders (McIver and Evans (1985)), submerged obstacles with arbitrary shapes (Dias and Vanden-Broeck (1989, 2004)), open channels (Evans and Linton (1991)) and a row of circular cylinders (Utsunomiya and Eatock Taylor (1999)), among others. See Ursell (1987) for a mathematical discussion of trapped modes in the linear theory of surface waves. Linton and Evans (1991) and Parsons and Martin (1995), for example, study the formation of the trapped modes above a submerged horizontal plate, within the linear water wave theory assumption. For further discussion on trapped waves, see for example a survey book by Kuznetsov et al. (2002), Chapter 5.

To quantify wave scattering by a submerged plate, and compare the GN results with results of laboratory experiments and other theoretical solutions, we shall define reflection and transmission coefficients for the GN equations. These coefficients use the change in wave height upwave and downwave to represent the energy reflection and attenuation. The plate results in wave scattering and formation of higher harmonics upwave and downwave. To define reflection and transmission coefficients, the main (fundamental) wave should be distinguished from the additional components and the locked modes.

A number of methods are suggested to determine the ratios of reflected and transmitted wave amplitudes to the incident wave amplitude, namely reflection and transmission coefficients. In a method suggested by Goda and Suzuki (1976), linear wave surface elevation recorded by two adjacent gauges are considered. The amplitudes of the reflected and transmitted waves are then estimated by use of the Fourier transform method. A similar approach, based on recordings of three wave gauges is discussed by Mansard and Funke (1980), where the least square method is used to calculate the coefficients. The methods suggested by Goda and Suzuki (1976) and Mansard and Funke (1980), however, cannot distinguish between the free and phase-locked modes. To overcome this problem, a method is proposed by Brossard et al. (2000) and Brossard and Chagdali (2001), in which the gauges upwave and downwave of the obstacle move with constant speed with respect to a fixed point. Such configuration allows for determination of the doppler effect. The free and locked modes of oscillation are distinguished by calculating the autospectrum of the recorded surface elevation by each moving probe.

In this study, we will use a four-gauge (two gauges upwave and two gauges downwave) method, introduced by Grue (1992), to distinguish the free and locked components and define the reflection and transmission coefficients. In this approach, first the nonlinear wave is decomposed into a series of linear components by use of the Fourier transform.

Here, we summarize this method with respect to the problem of wave interaction with a submerged plate. Upwave of the plate, the surface elevation η_{up} consists of the surface elevation of the incoming wave η_I and the surface elevation of the reflected wave η_R

$$\eta_{up}(x_1,t)=\eta_I(x_1,t)+\eta_R(x_1,t), \qquad x_1<X_L, \tag{28}$$

assuming the interaction of the incident and reflected waves do not lead into generation of any oscillation modes.

We assume that the surface elevation of the incoming wave η_I with amplitude a_I, wave number k and wave frequency ω, can be decomposed into free and bound (phase-locked) harmonics as

$$\eta_I = \left(\eta_{If}\right) + \sum_{n=2}^{N}\left[\eta_{If}^{(n)} + \eta_{Ib}^{(n)}\right] = \tag{29a}$$

$$= a_I \cos(kx_1 - \omega t + \phi) + \sum_{n=2}^{N}\left[a_{If}^{(n)} \cos(k_n x_1 - n\omega t + \phi_f^{(n)})\right] + \sum_{n=2}^{N}\left[a_{Ib}^{(n)} \cos n(kx_1 - \omega t + \phi)\right],$$

where $a_{If}^{(n)}$ and $a_{Ib}^{(n)}$ denote the amplitude of the free and bound n^{th} harmonic wave component, respectively, ϕ is the phase angle of the fundamental wave, k_n and $\phi_f^{(n)}$ are the wave number and phase angle of the n^{th} harmonic incoming free wave component. The bound harmonics are connected to the fundamental incoming wave component. The wave numbers of the free harmonic wave components are given by the linear dispersion relation:

$$(n\omega)^2 = g k_n \tanh k_n h\,, \qquad n = 1, 2, 3, \ldots\,. \tag{30}$$

We use $n = 1$ for the fundamental wave. The waves reflected from the obstacle are assumed to be decomposed similarly by

$$\eta_R = \left(\eta_{Rf}\right) + \sum_{n=2}^{N}\left[\eta_{Rf}^{(n)} + \eta_{Rb}^{(n)}\right] = \tag{31a}$$

$$= a_R \cos(kx_1 + \omega t + \phi_R) + \sum_{n=2}^{N}\left[a_{Rf}^{(n)} \cos(k_n x_1 + n\omega t + \phi_{Rf}^{(n)})\right] + \sum_{n=2}^{N}\left[a_{Rb}^{(n)} \cos n(kx_1 + \omega t + \phi_R)\right],$$

where a_R is the first harmonic reflected free wave amplitude, $a_{Rf}^{(n)}$ is the free n^{th} harmonic reflected wave amplitude, and $a_{Rb}^{(n)}$ denotes the amplitude of the bound n^{th} harmonic wave components connected to $a_R \cos(kx_1 + \omega t + \phi_R)$. ϕ_R is the phase angle of the first harmonic reflected wave, and $\phi_{Rf}^{(n)}$, $n = 2, 3, \ldots$, are the phase angles. Note that the reflected waves move to the opposite direction of the incoming wave *i.e.*, they are left going.

Similarly, the surface elevation of the transmitted waves η_T is assumed to be composed of free and bound (phase-locked) harmonics as

$$\eta_T = \left(\eta_{Tf}\right) + \sum_{n=2}^{N}\left[\eta_{Tf}^{(n)} + \eta_{Tb}^{(n)}\right] = \tag{32a}$$

$$= a_T \cos(kx_1 - \omega t + \phi_T) + \sum_{n=2}^{N}\left[a_{Tf}^{(n)} \cos(k_n x_1 - n\omega t + \phi_{Tf}^{(n)})\right] + \sum_{n=2}^{N}\left[a_b^{(n)} \cos n(kx_1 - \omega t + \phi_T)\right],$$

where a_T is the first harmonic transmitted free wave amplitude, $a_{Tf}^{(n)}$ is the free n^{th} harmonic transmitted wave amplitude, and $a_{Tb}^{(n)}$ denotes the amplitude of the n^{th} harmonic wave components connected to $a_T \cos(kx_1 - \omega t + \phi_T)$. ϕ_T is the phase angle of the first harmonic transmitted wave, and $\phi_{Tf}^{(n)}$, $n = 2, 3, \ldots$, are the phase angles. The transmitted waves are right-going, *i.e.*, in the same direction as the incoming wave.

Once the free and bound wave components of the incident, reflected and transmitted waves are distinguished, the reflection and transmission coefficients can be defined as the ratio of the wave amplitudes of the first harmonics, or higher free or bound harmonics.

In this approach, we use four wave gauges, namely GI, GII, GIII, and GIV, to record the surface elevation $\eta(x_1, t)$. Gauges GI, and GII are located upwave of the plate at $x_1 = X_I$ and $x_1 = X_I + \Delta X_I$, respectively, where ΔX_I is the distance between the two gauges upwave. Gauges GIII, and GIV are located downwave of the plate at $x_1 = X_{II}$ and $x_1 = X_{II} + \Delta X_{II}$, respectively, where ΔX_{II} is the distance between the two gauges downwave. The relative location of the gauges are shown in Fig. 1. No restrictions are placed on the ΔX_I and ΔX_{II} distances in this method.

Assuming that the surface elevation recorded by the gauges can be decomposed into free and bound components, in the form of Eqs. (31a) and (32a), the free waves are then determined by use of the Fourier transform given by

$$\hat{\eta}^{(n)}(x_1) = \frac{\omega}{2\pi}\int_0^{\frac{2\pi}{\omega}} \eta(x_1,t)e^{-in\omega t}dt, \qquad n = 1,2,3,\ldots, \tag{33}$$

where $i = \sqrt{-1}$. We will use the dispersion relation of the linearized Level I GN equations, given by Green et al. (1974) as

$$\omega^2 = \frac{ghk^2}{1+\frac{1}{3}(h^2k^2)}. \tag{34}$$

The fundamental amplitude of the incident wave, a_I, and the amplitude of the first harmonic of the reflected wave, a_R, can be discerned using $\hat{\eta}^{(1)}(x_1)$ from (33) by

$$a_I = \frac{1}{|\sin(k\Delta X_I)|}|\hat{\eta}^{(1)}(X_I) - \hat{\eta}^{(1)}(X_I+\Delta X_I)e^{-ik\Delta X_I}|, \tag{35a}$$

$$a_R = \frac{1}{|\sin(k\Delta X_I)|}|\hat{\eta}^{(1)}(X_I) - \hat{\eta}^{(1)}(X_I+\Delta X_I)e^{ik\Delta X_I}|. \tag{35b}$$

Similarly, the amplitude of the transmitted fundamental free wave is obtained through the recordings of GIII and GIV gauges by

$$a_T = \frac{1}{|\sin(k\Delta X_{II})|}|\hat{\eta}^{(1)}(X_{II}) - \hat{\eta}^{(1)}(X_{II}+\Delta X_{II})e^{-ik\Delta X_{II}}|. \tag{36a}$$

The amplitudes of the higher harmonics of the free and locked reflected waves can be calculated similarly by

$$a^{(n)}_{Rb} = \frac{2}{|\sin(k_n - nk)\Delta X_I|}|\hat{\eta}^{(n)}(X_I) - \hat{\eta}^{(n)}(X_I+\Delta X_I)e^{-ink\Delta X_I}|, \qquad n = 2,3,4,\ldots \tag{37a}$$

$$a^{(n)}_{Rf} = \frac{2}{|\sin(k_n - nk)\Delta X_I|}|\hat{\eta}^{(n)}(X_I) - \hat{\eta}^{(n)}(X_I+\Delta X_I)e^{-ik_n\Delta X_I}|, \qquad n = 2,3,4\ldots. \tag{37b}$$

Once the amplitudes of the incident, reflected and transmitted waves are determined, the reflection and transmission coefficients can be calculated. In this study, the reflection coefficient, C_R, is defined as the ratio of the first harmonic of the reflected wave amplitude, a_R, to the fundamental (incident) wave amplitude, a_I:

$$C_R = \frac{a_R}{a_I}. \tag{38}$$

The transmission coefficient, C_T, is defined as the ratio of the first harmonic of the transmitted wave amplitude, a_T, to a_I:

$$C_T = \frac{a_T}{a_I}. \tag{39}$$

It is possible to define the reflection and transmission coefficients for the higher bound or free harmonics, see, for example, Liu et al. (2009). Here, however, we shall only focus on the fundamental harmonic. Consequently, the relation $C_R^2 + C_T^2 = 1$, applicable to linear waves, is not always exactly satisfied for nonlinear wave transformation using the above definition of C_R and C_T coefficients. In principle, further information on the wave scattering can be obtained by considering evolution of the higher harmonics of the reflected and transmitted waves. See, *e.g.*, Gobbi and Kirby (1999) for spatial variation of the Fourier components of the free surface elevation of nonlinear wave evolution over submerged sills.

We note that this approach in reconstructing the nonlinear GN results by use of the Fourier transform is used here to define the reflection and transmission coefficients. To examine this decomposition, the GN surface elevation of a small-amplitude wave ($H/h = 0.067$ and $\lambda/L_p = 2.5$) recorded in Gauges I and III, upwave and downwave of a submerged plate ($d/h = 0.33$ and $L_p/h = 2.0$) are recreated by use of the Fourier transform

$$\eta(x_1,t) = \sum_{n=1}^{N} a^{(n)}\cos\left(n\omega t - \phi^{(n)}\right), \tag{40}$$

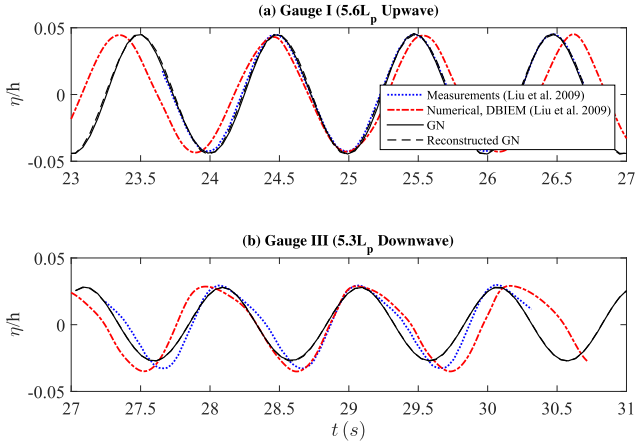

FIG. 2. Comparison of results of the GN equations of wave scattering over a submerged horizontal plate, with the laboratory measurements and computations of Liu et al. (2009). The decomposed GN surface elevation, using Eq. (40), is in excellent agreement with the original GN results, and both are in good agreement with the laboratory measurements. $H/h = 0.067$, $d/h = 0.33$, $L_p/h = 2.0$, $\lambda/h = 2.5$.

where $a^{(n)}$ is the amplitude of the n^{th} harmonic wave, ω is the angular frequency of the fundamental (first harmonic) incident wave calculated by Eq. (34), and $\phi^{(n)}$ are the phase angles.

The original GN and the reconstructed waves are show in Fig. 2. A curve fitting technique (the nonlinear least-squares solver of MATLAB) is applied to determine the unknown amplitudes and the phase angles. In this case, the series of Eq. (40) converges at $N = 3$. The reconstructed GN curve is on top of the original GN results. Surface elevations are in good agreement with the laboratory measurements and numerical results of Liu et al. (2009).

The approximation error associated with the wave decomposition would increase for long waves in shallow water. A fundamental source of error in using this approach to decompose the GN results (with finite number of sentences) is that, in the case of cnoidal waves, a larger mass of the wave is above the SWL, unlike in linear waves. We shall use this method to compare the GN results for the reflection and transmission coefficients with the laboratory measurements and existing numerical solutions in the literature, given in Section IV, where only intermediate-to deep-water waves are considered.

For consistency, throughout this paper, Gauges I and II are upwave of the plate, and Gauges III and IV are downwave. Gauges V and VI are above and below the plate, respectively, and at the centre.

IV. RESULTS AND DISCUSSION

Results of the GN equations for propagation of waves above a submerged plate are given in this section. The GN results are compared with the laboratory measurements and other theoretical solutions when possible.

A snapshot of the numerical wave tank of the Level I GN equations for the interaction of cnoidal waves ($H/h = 0.2$) with a horizontal plate ($L_p/h = 20$), submerged at $d/h = 0.5$ in shallow water ($\lambda/h = 40$) is shown in Fig. 3.

The incoming cnoidal waves undergo significant deformation due to the plate, mainly by the wave-wave effect, and partially due to the wave-structure effect. Upwave from the plate, the reflected wave (left-going) interacts with the incoming wave (right-going) and causes some deformations of it. Above the plate, due to the sudden change of the water depth, the wave height increases and the wave profile steepens, see the wave crest approaching the trailing edge of the plate in Fig. 3. In this specific case, the wave face at the trailing edge of the plate is so steep that the wave is nearly breaking. Above the plate, trailing waves are generated and separated from the main wave crest as they propagate in the shallow region. Downwave of the plate, the waves undergo further deformation due to the sudden increase in the water depth. The trailing waves are distinguished from the main crest, and the height of the main wave is noticeably smaller.

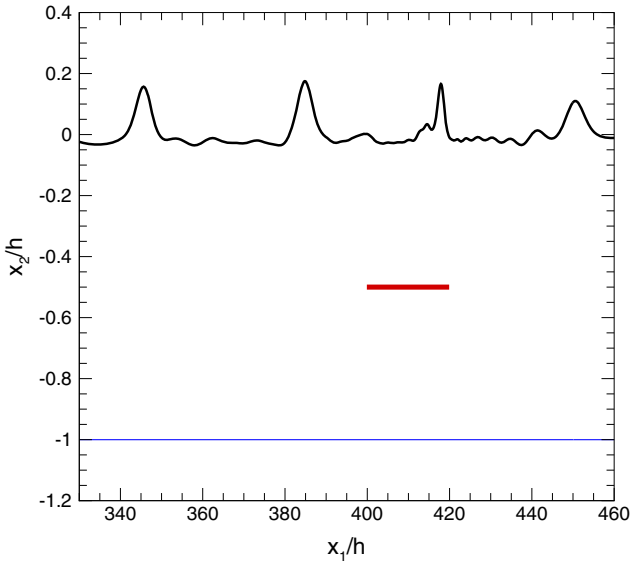

FIG. 3. Snapshot of interaction of cnoidal waves with the submerged, thin plate calculated by the GN equations. $H/h = 0.2$, $d/h = 0.5$, $L_p/h = 20$, $\lambda/h = 40$.

This wave scattering process can also be seen in Fig. 4, where the surface elevation and horizontal velocity are recorded at five gauges. In this figure, Gauge I is at the wavemaker ($x_1 = 0$) recording the un-scattered incident wave, Gauge II is one plate length upwave from the leading edge ($x_1 = X_L - L_p$), Gauges V and VI are at the center, above and below the plate, respectively ($x_1 = X_L + L_P/2$), and Gauge III is one plate length downwave from the trailing edge of the plate ($x_1 = X_T + L_P$). The wave condition and plate characteristics are the same as those in Fig. 3.

While the wave propagates above the plate, there is a pulsating flow underneath the plate. Shown in Fig. 5, pressure varies linearly under the plate between the leading and trailing edges of the plate, the vertical velocity is zero, and hence there is a spatially-invariant uniform flow under the plate.

A. Results comparison

Results of the GN equations for wave scattering by a submerged plate are compared with existing laboratory experiments and other theoretical solutions in this section.

Comparison of the results of the GN equations with the laboratory measurements and computational results of Euler's equations by Hayatdavoodi et al. (2015) of the time series of cnoidal wave scattering by a submerged plate is shown in Fig. 6. Overall, a close agreement is observed between

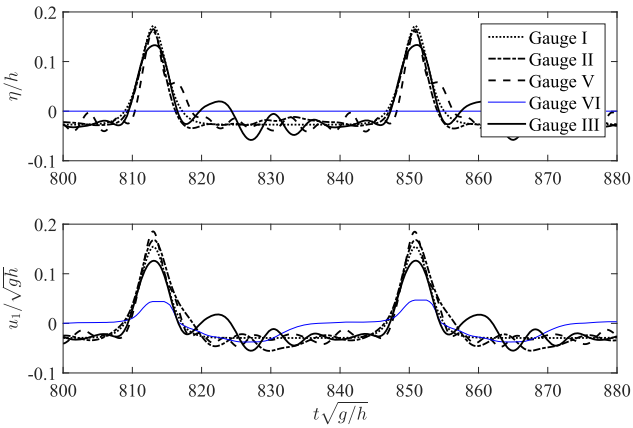

FIG. 4. Surface elevation and horizontal velocity of cnoidal wave interaction with a submerged plate, recorded by five gauges. Location of the gauges are given in the text. $H/h = 0.2$, $d/h = 0.5$, $L_p/h = 20$, $\lambda/h = 40$.

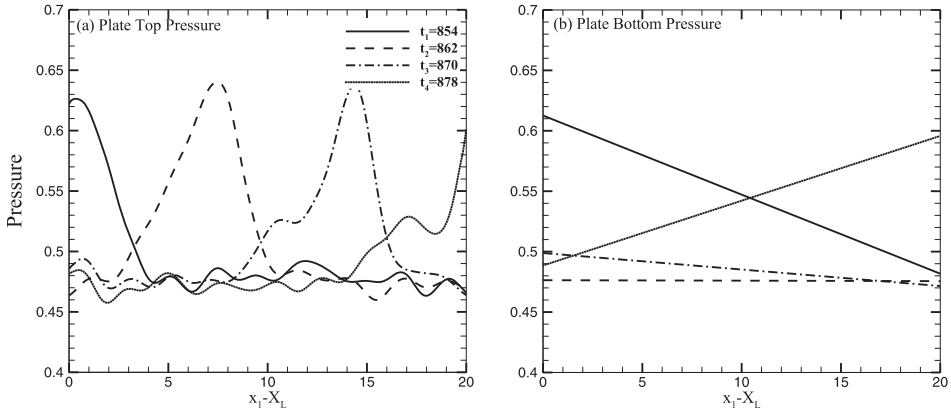

FIG. 5. Cnoidal wave pressure (a) above and (b) below the submerged plate, calculated by the GN equations. The pressure is dimensionless as Pressure $= \frac{p}{\rho g h}$, where p is the dimensional (total) pressure. Times are dimensionless as $t_1 = t\sqrt{g/h}$, and similarly for t_2, t_3 and t_4. $H/h = 0.2$, $d/h = 0.5$, $L_p/h = 20$, $\lambda/h = 40$.

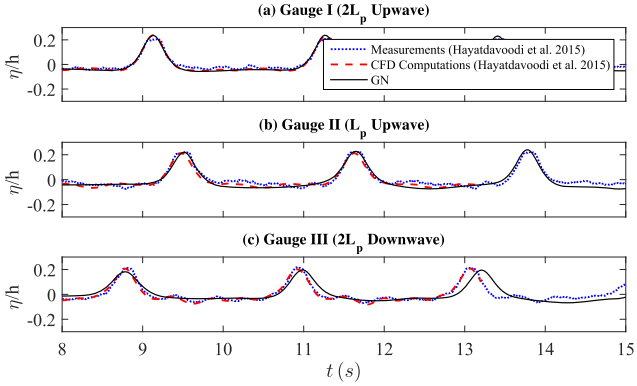

FIG. 6. Comparison of results of the GN equations with the laboratory measurements and Euler's equations results of Hayatdavoodi et al. (2015). $H/h = 0.3$, $d/h = 0.6$, $L_p/h = 2.102$, $\lambda/h = 26.7$.

results of the GN equations with Euler's equations and laboratory measurements. The GN transmitted wave, recorded in gauge III shown in Fig. 6(c), shows less fluctuation at the wave trough, and slightly slower propagating waves when compared with the other results. The wave height of the main wave, however, is in close agreement.

Next, comparison of the reflected and transmitted coefficients of the GN results, calculated by Eq. (38) and Eq. (39), respectively, with existing laboratory measurements and theoretical solutions are presented. For a given inviscid fluid, the reflection and transmission coefficients vary with wave conditions and plate characteristics, *i.e.*, $C_T = f_T(h, H, \lambda, d, L_p)$, and similarly $C_R = f_R(h, H, \lambda, d, L_p)$, where f_T and f_R are unknown functions. All the variables have length dimension, and hence dimensionless parameters can be formed by grouping any two parameters to study the variation of C_R and C_T.

In this section, the wave conditions and plate characteristics (plate length and the submergence depth) follow the existing data in the literature, so that the results of the GN equations can be compared. We note that in the literature, different methods are used to define the reflection and transmission coefficients. Agreement between the results (C_R and C_T) of the GN equations and the data in the literature depends on the agreement in predicting the wave field, as well as (to some degree) the method used in determining the coefficients themselves.

Variation of the reflection and transmission coefficients with the $kh(= 2\pi/\lambda h)$ parameter is shown in Fig. 7, where wavelength is the variable. The coefficients vary nonlinearly with the kh parameter, with distinguished peaks and troughs. The plate has a more significant effect on the wave field for smaller kh values, corresponding to shallow water regions. The oscillatory nonlinear variation of the coefficients with the kh parameter suggests that other parameters (plate length, in this case) also

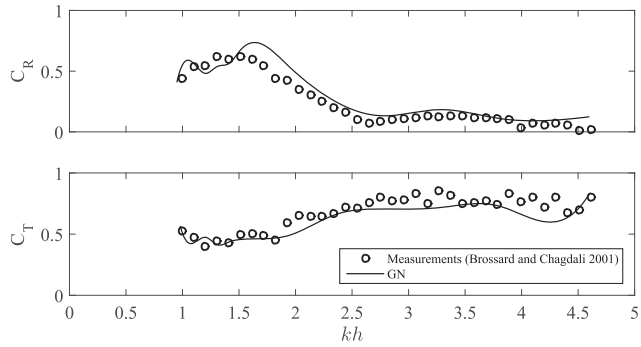

FIG. 7. Periodic wave scattering by a submerged plate vs. kh parameter. Comparison of the reflection coefficient (C_R) and the transmission coefficient (C_T) of the GN equations with the laboratory measurements of Brossard and Chagdali (2001). $H/h = 0.11$, $L_p/h = 1.33$, $d/h = 0.24$, and λ is variable.

play a significant role on wave scattering. Overall, a close agreement between the GN results and laboratory measurements of Brossard and Chagdali (2001) is observed.

Variation of the reflection and transmission coefficients with the wavelength over plate length ratio, λ/L_p, for a relatively small wave ($H/h = 0.067$) is shown in Fig. 8. In this figure, the submergence depth is $d/h = 0.33$ and plate length is $L_p/h = 2.0$, and these are kept constant. The reflection coefficient, C_R, initially increases with λ/L_p values up to $\lambda/L_p \approx 2.7$, and then it shows some small reduction for longer waves. Conversely, the transmission coefficient, C_T, shows an initial reduction with larger λ/L_p up to $\lambda/L_p \approx 2.7$, and then becomes slightly larger for longer waves. For relatively shorter waves, the plate has less effect on wave scattering. These results, for the maximum and minimum wave reflection and transmission, are in close agreement with the laboratory measurements of Dattatri et al. (1977) on optimum plate length for maximum reflection from a submerged breakwater ($\lambda/L_p \approx 2.5 - 3.3$) in intermediate-depth wave conditions.

Shown in Fig. 8, overall, a close agreement is observed between the GN results and laboratory measurements of Liu et al. (2009), particularly for longer waves. Good agreement is observed with the computational results of Liu et al. (2009) and Lin et al. (2014), who used a boundary-element method and a desingularized boundary integral equation method, respectively. See Cao et al. (1991) for information on the latter method. The long-wave approximation analytical results of Siew and Hurley (1977) is also included in Fig. 8. The LWA results are not in agreement with other results, particularly for shorter waves. The reflection coefficient calculated by the method of Siew and Hurley (1977) is

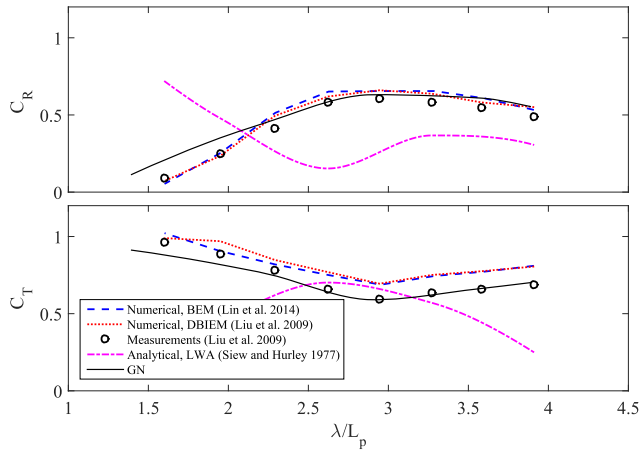

FIG. 8. Periodic wave scattering by a submerged plate vs. λ/L_p ratio. Comparison of the reflection coefficient (C_R) and the transmission coefficient (C_T) of the GN equations and laboratory measurements of Liu et al. (2009), numerical results of Liu et al. (2009) and Lin et al. (2014), and analytical results of Siew and Hurley (1977). $H/h = 0.067$, $d/h = 0.33$, $L_p/h = 2.0$, and λ is variable.

roughly in better agreement than the transmitted coefficient is. The main reason for the discrepancy between Siew and Hurley's method and other results is the assumption of long plate length (L_p/h), which is not applicable in this case, where ($L_p/h = 2.0$). Moreover, the relatively smaller submergence depth ($d/h = 0.33$) in this case poses further challenge to the assumptions made to drive the LWA solution. Such discrepancy is observed between the LWA results and other results in cases studied hereafter. Hence, only the reflection coefficient of the LWA is included, which is comparable to other results. Further discussion on the applicability of the method of Siew and Hurley (1977) for different wave conditions can be found in Patarapanich (1978, 1984), who used the analytical solution of Siew and Hurley (1977) to obtain the condition for maximum and zero wave reflection due to a submerged plate.

Variation of the reflection and transmission coefficients with λ/L_p ratio for a plate submerged in the middle of the water depth, $d/h = 0.5$, is shown in Fig. 9. Shown in this figure, the reflection and transmission coefficients vary less with the λ/L_p ratio when compared with the results shown in Fig. 8, where the plate was closer to the SWL ($d/h = 0.33$). Note that the wave condition of Fig. 9 is slightly different from those in Fig. 8. The variation of the coefficients with the λ/L_p ratio, however, is in overall agreement with Fig. 8, in that a peak reflection coefficient can be observed for $\lambda/L_p \approx 2.7$.

Overall, a close agreement is observed between the results of the GN equations and the laboratory experiments of Brossard et al. (2009), and the BEM solution of Liu et al. (2009) and the DBIEM solution of Lin et al. (2014). For this case of a plate submerged at deeper depth ($d/h = 0.5$), LWA results for the reflection coefficient is in closer agreement with other data. Results of the theoretical approaches are in closer agreement with the laboratory measurements for the reflection coefficient when compared with the transmission coefficient. This is partially due to the extreme wave transformation in the shallow region over the submerged plate where the theoretical solutions show some differences. Wave reflection, however, mainly occurs as the wave approaches the leading edge of the plate, and due to the sudden change in the water depth above the plate. Viscosity of the fluid, neglected in all theories of Fig. 9, may also play a small role on the transmitted wave; a small part of the energy is dissipated due to the skin friction and formation of the vortices.

Shown in Fig. 9, the GN equations have slightly underestimated the transmission coefficient, while other theoretical solutions have overestimated it, when results are compared with the laboratory measurements. Given the value of the reflection coefficient for most of the wavelengths ($C_R \approx 0.2$), results of the GN equations seem more physical than the other theoretical results, which have predicted $C_T \approx 1$.

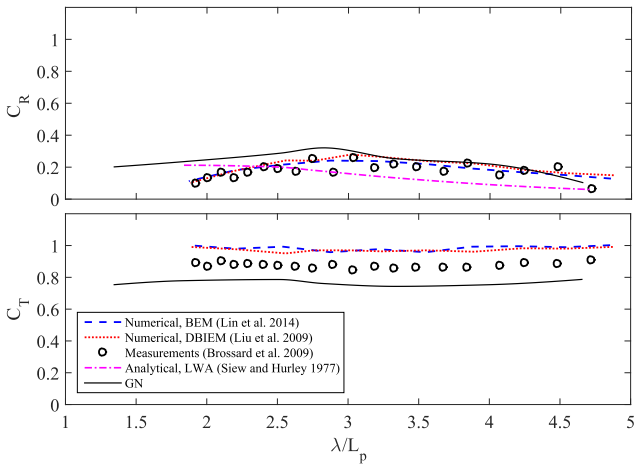

FIG. 9. Periodic wave scattering by a submerged plate vs. λ/L_p ratio. Comparison of the reflection coefficient (C_R) and the transmission coefficient (C_T) of the GN equations and laboratory measurements of Brossard et al. (2009), numerical results of Liu et al. (2009) and Lin et al. (2014), and analytical results of Siew and Hurley (1977). $H/h = 0.1$, $d/h = 0.5$, $L_p/h = 1.25$, and λ is variable.

In Fig. 10, variation of the wave transformation by a submerged plate with the λ/L_p ratio for three submergence depths d/h = 0.24, 0.48 and 0.74 are shown. In this figure, the wave height (H/h = 0.11) and plate length (L_p/h = 1.33) are kept constant, while the wavelength (λ) is variable. The reflection and transmission coefficients show an oscillatory behavior for $1 < \lambda/L_p < 2$. This is when the wavelength is comparable with the plate length, *i.e.* the wave crest and wave trough may be located at the leading and trailing edges of the plate simultaneously. As the wavelength increases, the coefficients show less variation.

In all cases, shown in Fig. 10, the reflection coefficient approaches a maximum value at $\lambda/L_p \approx 2.7-3.0$, similar to that discussed for Figs. 8 and 9. The transmission coefficient reaches a minimum value at this point, and this is not remarkable. Variation of the coefficients with the λ/L_p ratio is significantly higher when the plate is closer to the surface. As the plate moves into deeper water, the coefficients become invariant with the λ/L_p ratio. For the largest submergence depth ($d/h = 0.74$), the reflection coefficient approaches zero and transmission coefficient approaches one for longer waves. A close agreement between the GN results and the laboratory measurements of Brossard et al. (2000) is observed. The agreement is better when the plate is submerged at a deeper depth and for longer waves. The LWA results are in better agreement with the data as the submergence depth increases.

To further analyze the effect of submergence depth on the reflection and transmission coefficients in Fig. 11, the wave conditions, H/h = 0.1 and $\lambda/h = 3.125$, and the plate length, L_p/h = 1.25, are kept constant and the plate is submerged at different depths. Shown in this figure, and similar to the behavior seen in Fig. 10, the reflection coefficient decreases continuously with the submergence depth, while the transmission coefficient increases. The submergence depth has a less important effect on the wave transformation at about $d/h \approx 0.5$ and beyond. Very close agreement between the GN results and the laboratory experiments of Brossard et al. (2009) is observed. As expected, the plate has less effect on wave transformation when it is submerged at deeper depths. As $d/h \to 1$, $C_R \to 0$ and $C_T \to 1$.

B. Shallow-water cnoidal wave scattering

In the previous subsection, and for comparison with laboratory experiments and results of other theoretical approaches, the plate in all cases was located in intermediate or deep waters. In this

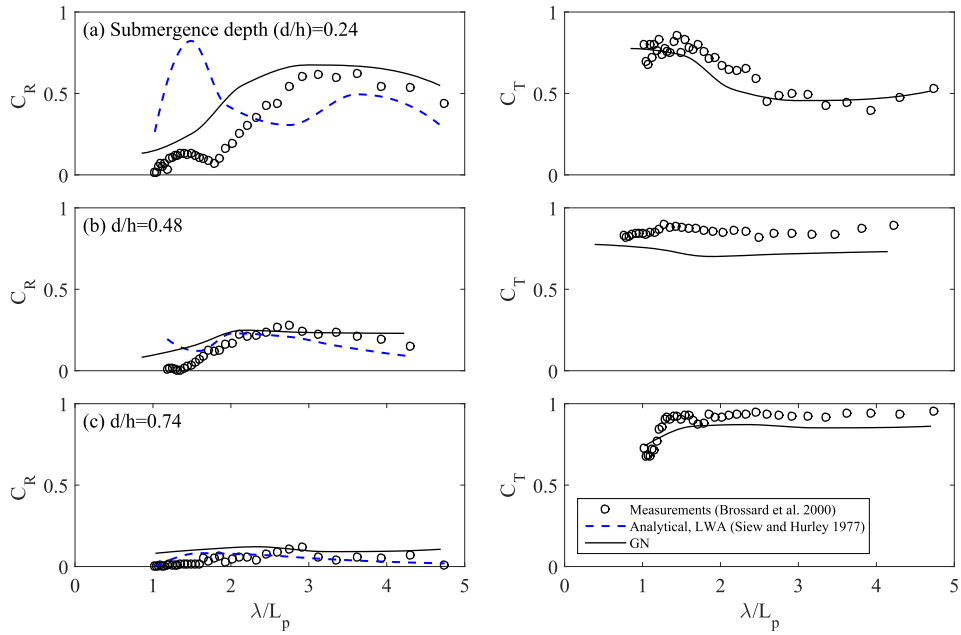

FIG. 10. Variation of the reflection coefficient (C_R) and the transmission coefficient (C_T) with λ/L_p ratio, for plates submerged at (a) d/h = 0.24, (b) d/h = 0.48, and (c) d/h = 0.74; comparison of results of the GN equations with laboratory measurements of Brossard et al. (2009) and analytical results of Siew and Hurley (1977). H/h = 0.11, L_p/h = 1.3, and λ is variable.

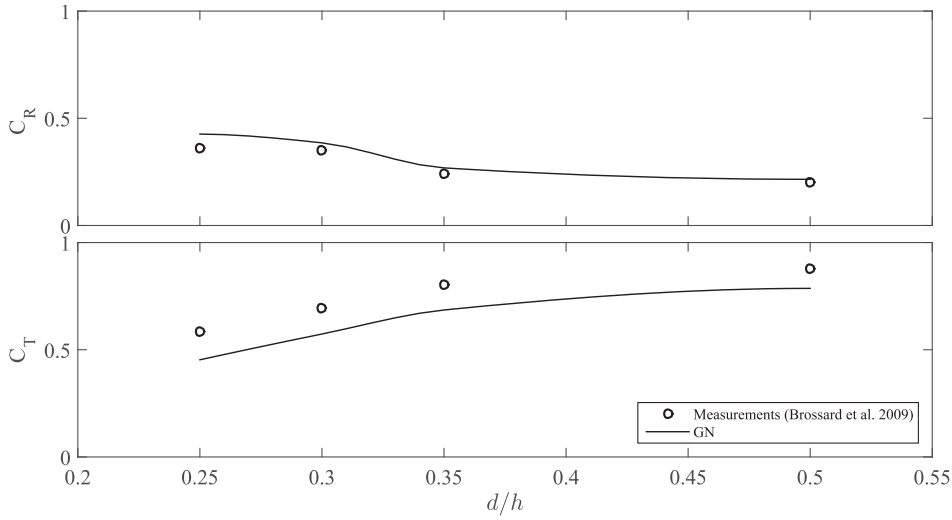

FIG. 11. Periodic wave scattering by a submerged plate vs. d/h ratio. Comparison of the reflection coefficient (C_R) and the transmission coefficient (C_T) of the GN equations with the laboratory measurements of Brossard et al. (2009). $H/h = 0.1$, $\lambda/h = 2.5$, $L_p/h = 1.25$, and d is variable.

subsection, we will study the effect of the plate on long-waves scattering when it is locate in shallow water. The default wave condition of $H/h = 0.2$ and $\lambda/h = 20$ and plate characteristic of $L_p/h = 6.7$ and $d/h = 0.4$ are used in all cases of this subsection. In each case, the nonlinear wave transformation is studied by changing one parameter, while keeping others constant.

In this section, the surface elevation (η/h) is recorded at four wave gauges: Gauge I at the location of the wavemaker (un-scattered incident wave), Gauge II five plate lengths upwave of the plate leading edge, Gauge V above the plate at the center, and Gauge III five plate lengths downwave of the trailing edge of the plate. Time series of the dimensionless surface elevation (η/h), recorded by the gauges are given in all cases.

Figure 12 shows the time series of the nonlinear wave transformation due to a submerged plate for different wave heights. Four wave heights are considered in this figure: $H/h = 0.1$, 0.2, 0.3 and 0.4. The plate has more significant impact on the wave for larger waves. For smaller waves, *e.g.* Fig. 12(a), some deformation of the wave is observed at Gauge V, above the plate. The wave, however, recovers its form when propagates downwave of the plate, see Gauge III of Fig. 12(a). This is not the case for larger wave heights, see Fig. 12(d), where Gauge III downwave shows remarkable scattering of the wave, and the wave height is significantly reduced.

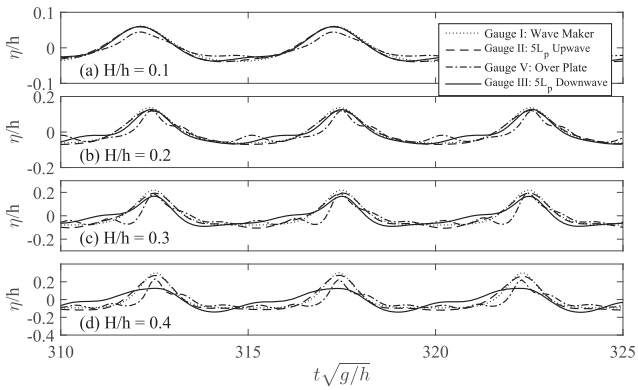

FIG. 12. Time series of cnoidal wave scattering by a submerged plate, calculated by the GN equations, for (a) $H/h = 0.1$, (b) $H/h = 0.2$, (c) $H/h = 0.3$, and (d) $H/h = 0.4$. Other parameters are constant: $d/h = 0.4$, $L_p/h = 6.7$, $\lambda/h = 20$.

Seen in Gauge V of 12(b), over the plate at the center, a second hump is clearly formed in between the two consecutive wave crests; see times $\bar{t} = t\sqrt{g/h} \approx 315$ an $\bar{t} \approx 320$ of this figure. As the wave height increases, in Figs. 12(c) and (d), the height of this second hump drops. However, two other distinguished humps appear in between the two consecutive wave crests. As the incident wave height increases, for a fixed submergence depth, the wave diffraction above the plate is stronger, *i.e.*, the initial increase in the wave height above the plate occurs faster, and as the wave propagates in the shallow region, extra humps form and separate from the main crest. Hence, the height of the main wave, recorded at the center of the plate, drops with the increase in the incident wave height.

Figure 13 shows the time series of nonlinear wave transformation by a submerged plate in shallow water for different λ/L_p ratios. In this figure, to allow a comparison between cases with different λ/L_P ratios, the wavelength is kept constant ($\lambda/h = 20$) and the plate length is varied. The plate length is decreasing from Fig. 13(a) to Fig. 13(d). As expected, the longer plates cause more significant wave scattering. The effect of the plate length on wave scattering, however, remains nonlinear for shallow-water waves. For $\lambda/L_p = 0.5$, Fig. 13(a), the reflected wave has caused a deeper trough upwave, while a small second hump is generated downwave. For $\lambda/L_p = 2$, Fig. 13(c), however, Gauge III downwave shows the largest reduction in the elevation of wave crest from the SWL among cases considered in this figure. Note the increase of the elevation of the wave crest, above the plate, compared with the incoming wave, particularly seen in Fig. 13(c), Gauge V.

These results are in qualitative agreement with those discussed in Section IV for intermediate and deep water conditions. Overall, the plate length does not appear to have a significant effect on the scattering of long waves.

Time series of nonlinear wave transformation with plates located at different depths (d/h) in shallow water are shown in Fig. 14. Seen in this figure, the plate causes significant wave scattering when it is closer to the SWL. The plate has less effect as the submergence depth increases, but the relation remains nonlinear. This is in qualitative agreement with the results shown in Fig. 11, for intermediate to deep water conditions.

Comparison between results shown in Fig. 12, where the wave height is variable, with those shown in Fig. 14, where the submergence depth changes, shows that the plate submergence depth has a more important role on the wave scattering. In both Figs. 12(d) and 14(a), the ratio of the incident wave height to water depth above the plate is $H/d = 1$. The wave scattering caused by the plate in Fig. 14(d), however, is more significant particularly at the upwave region where the incoming wave has deformed more severely.

For the given wave height and plate length discussed in Fig. 14, wave breaking occurs at smaller submergence depths. Wave breaking above the plate results in energy attenuation and formation of higher harmonic oscillations. The transmission coefficient would reduce due to the wave breaking above the plate. For further discussion on the effect of wave breaking on the wave scattering see, e.g., Brossard and Chagdali (2001), who conducted laboratory experiments on wave interaction with

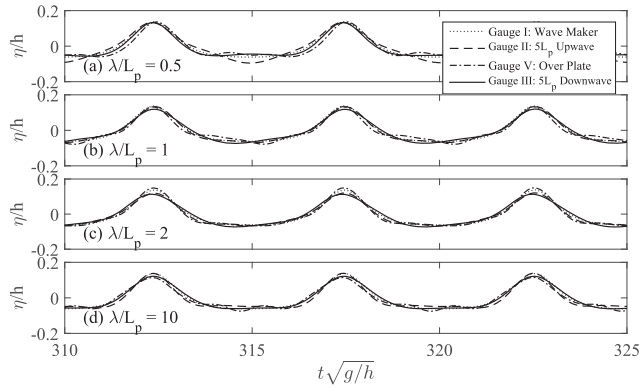

FIG. 13. Time series of cnoidal wave scattering by a submerged plate, calculated by the GN equations, for (a) $\lambda/L_p = 0.5$, (b) $\lambda/L_p = 1$, (c) $\lambda/L_p = 2$, and (d) $\lambda/L_p = 10$. Other parameters are constant: $H/h = 0.2$, $d/h = 0.4$, $L_p/h = 6.7$.

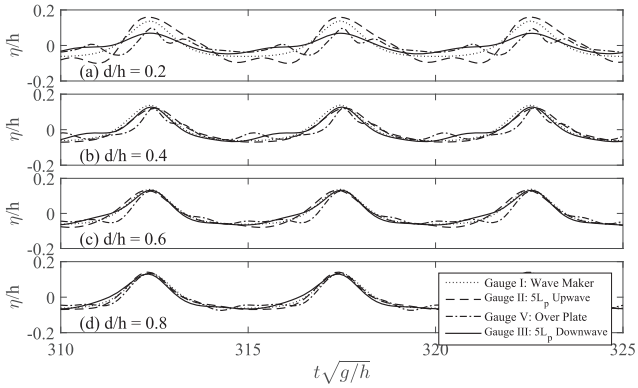

FIG. 14. Time series of cnoidal wave scattering by a submerged plate, calculated by the GN equations, for (a) $d/h = 0.2$, (b) $d/h = 0.4$, (c) $d/h = 0.6$, and (d) $d/h = 0.8$. Other parameters are constant: $H/h = 0.2$, $\lambda/h = 20$, $L_p/h = 6.7$.

a submerged plate. In general, the breaking limit of course depends on a combination of the wave height, wavelength to plate length ratio, and the submergence depth.

C. Solitary wave scattering

In this part, we study the transformation of a solitary wave propagating over a submerged plate calculated by the GN equations. After a discussion on the solitary wave scattering, the problem will be analyzed by studying the deformation of the surface elevation and by defining the reflection and transmission coefficients for the solitary wave.

Evolution of a solitary wave ($A/h = 0.2$) over a long plate ($L_p/h = 70$), submerged at $d/h = 0.4$ depth is shown in Fig. 15. The long plate, considered in this case, allows for a better observation of the solitary wave transformation over the plate. This figure consists of several snapshots of the numerical domain taken at constant time intervals. The solitary wave propagates from left to right, and in this figure, time increases from the top to bottom snapshots.

The solitary wave propagates with constant form and speed on the flat seafloor upwave from the plate. At time $\bar{t} = t_1$, approximately, the peak of the solitary wave approaches the leading edge of the plate (X_L). At this point, an oscillatory wave reflects back upwave, consisting of a series of waves with decaying wave heights. As the main soliton propagates above the plate, at time $t_1 < \bar{t} < t_2$, approximately, its height increases initially and a second soliton starts forming and separating from the main wave. The soliton fission process continues to develop until the peak of the main soliton approaches the trailing edge of the plate at time $\bar{t} = t_2$, approximately, after which the soliton moves from the shallow depth to deeper depth. Downwave from the plate, a series of oscillatory waves with decaying wave height are formed at the tail of the solitary wave, and the amplitude of the main

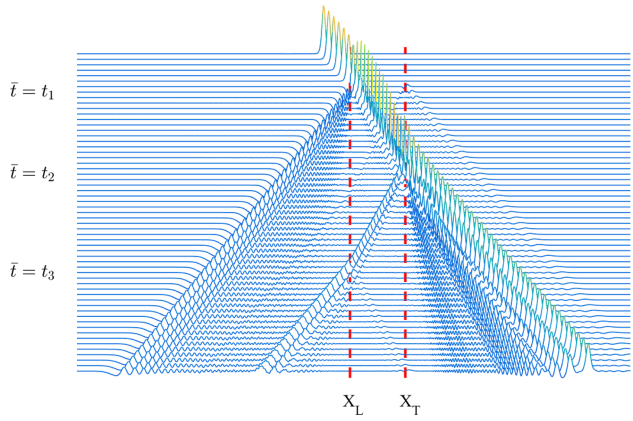

FIG. 15. Evolution of a solitary wave propagating over a submerged plate. The solitary wave moves from left to right, and location of the leading and trailing edges of the plate are shown by dashed lines. $A/h = 0.2$, $d/h = 0.4$ and $L_p/h = 70$.

soliton is decreased. Also seen at time $\bar{t} = t_2$, approximately, small wave reflection occurs as the main soliton propagates from shallow to deeper depth. The reflected waves propagate leftward over the submerged plate. Again, as the reflected wave approaches the leading edge of the plate, a wave with smaller amplitude is generated that travels back above the plate, this time, to the right, and this process continues. A portion of the energy is trapped above the plate and reflects back and forth between the leading and trailing edges, and it is attenuating. The propagation speed of the main soliton, and the waves above the plate vary when they travel in the deeper section of the domain versus above the plate, see times $\bar{t} = t_1$, $\bar{t} = t_2$, and $\bar{t} = t_3$, approximately, and this is not remarkable.

Also, in Fig. 15, note the surface fluctuations at the trailing edge of the plate, when the solitary wave approaches the leading edge of the plate at time $\bar{t} = t_1$, approximately. Similarly, small oscillations can be observed at the leading edge of the plate, when the main soliton approaches the trailing edge of the plate at time $\bar{t} = t_2$, approximately. These are due to the uniform flow under the plate, generated by the pressure differential at the leading and trailing edges, when the main soliton is at one end of the plate.

The above behaviour seen for the propagation of a solitary wave above the plate is somewhat similar to that of propagation of solitons above a submerged step or shelf, from deep to shallow section, and from shallow to deep section. Soliton fission occurs as the wave propagates to shallow depth above the shelf, and oscillatory waves separate from the main soliton as it propagates from shallow section to deeper depth. See, *e.g.*, Ertekin et al. (2014) for more details. Some distinguished differences are also apparent between these cases, mainly in the height of the humps and distances between them due to the oscillating flow under the plate.

A comparison of the results of the GN equations for propagation of a solitary wave above a submerged plate, with the laboratory measurements, and results of the Reynolds-Averaged Navier-Stokes (RANS) equations, and a linear solution of Lo and Liu (2014) is shown in Fig. 16. The propagation of the solitary wave is recorded at three gauges: Gauge I one plate length upwave, Gauge V above the plate at the centre, and Gauge III downwave form the plate. Overall, a close agreement is observed particularly between the GN results, and RANS results and the laboratory measurements. Some small differences are seen for the amplitude of the soliton above the plate at the centre.

Next, solitary wave transformation over a submerged plate recorded at four gauges in the numerical tank is presented here. The wave gauges are placed at the same locations as in the cnoidal wave cases: Gauge I is at the wavemaker, Gauge II is five plate length ($5L_p$) upwave from the leading edge, Gauge V is above the plate at the center, and Gauge III is $5L_p$ downwave of the plate trailing edge. Time series of the solitary wave transformation for different wave amplitude, plate length, and plate submergence depth are shown in Figs. 17, 18, and 19, respectively. In these figures, the horizontal time axis corresponds to the recordings of Gauge V above the plate. The recordings of the other gauges are shifted (in time) to match the wave in Gauge V, so that a comparison of the wave scattering at different gauges can be made. Gauge II, upwave from the plate, shows the main reflected hump. The

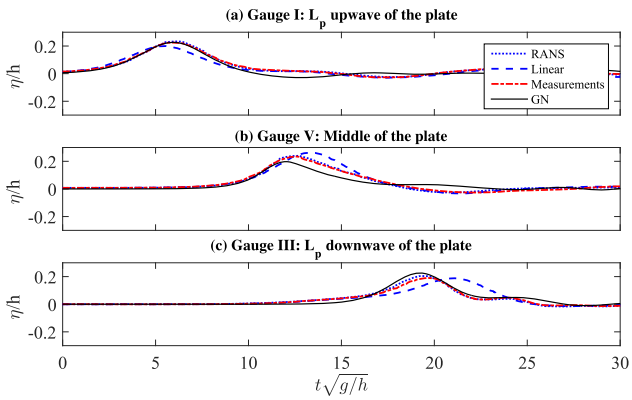

FIG. 16. Comparison of results of the GN equations, with the computations (RANS and Linear solutions) and laboratory measurements of Lo and Liu (2014), for propagation of a solitary wave above a submerged plate. $A/h = 0.2$, $d/h = 0.5$ and $L_p/h = 5.78$.

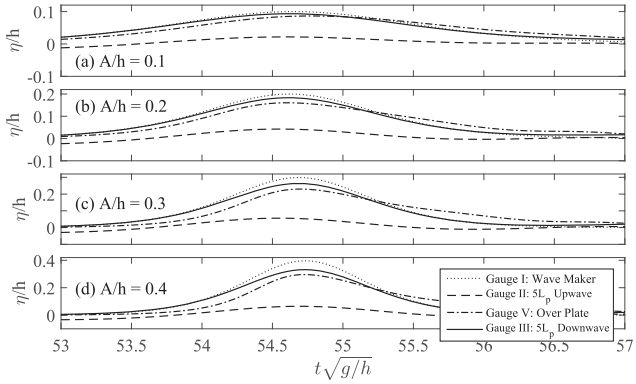

FIG. 17. Time series of solitary wave scattering by a submerged plate, calculated by the GN equations, for (a) $A/h = 0.1$, (b) $A/h = 0.2$, (c) $A/h = 0.3$, and (d) $A/h = 0.4$. Other parameters are constant: $d/h = 0.4$, $L_p/h = 2$.

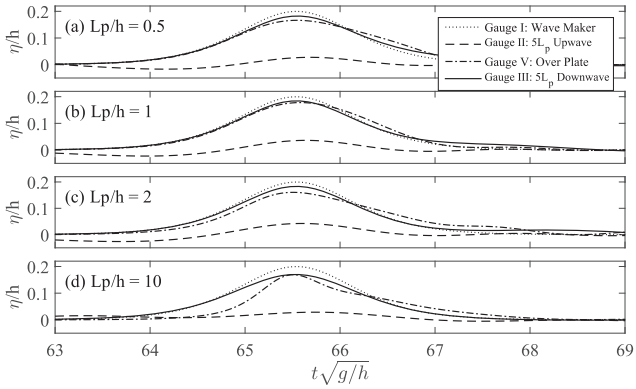

FIG. 18. Time series of solitary wave scattering by a submerged plate, calculated by the GN equations, for (a) $L_p/h = 0.5$, (b) $L_p/h = 1$, (c) $L_p/h = 2$, and (d) $L_p/h = 10$. Other parameters are constant: $A/h = 0.2$, $d/h = 0.4$.

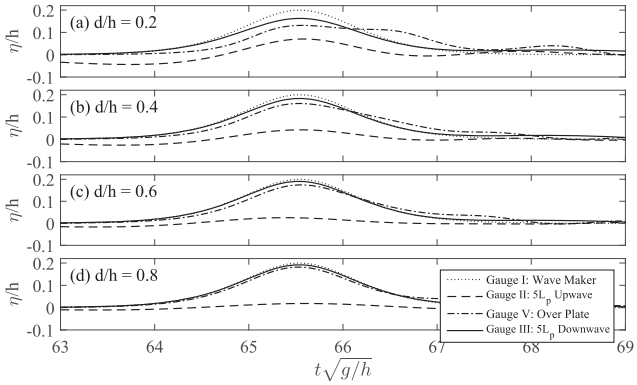

FIG. 19. Time series of solitary wave scattering by a submerged plate, calculated by the GN equations, for (a) $d/h = 0.2$, (b) $d/h = 0.4$, (c) $d/h = 0.6$, and (d) $d/h = 0.8$. Other parameters are constant: $A/h = 0.2$, $L_p/h = 2$.

default wave amplitude, $A/h = 0.2$, plate submergence depth, $d/h = 0.4$, and the plate length, $L_p/h = 2$, are used in this section. In Figs. 17, 18 and 19, one parameter is changed at a time, while other two parameters are fixed.

Figure 17 shows the solitary wave scattering of waves with variable amplitudes $A/h = 0.1$, 0.2, 0.3 and 0.4. The propagation speed of the GN solitary wave over a flat seafloor is calculated by $U = \sqrt{g(A+h)}$, see Ertekin and Wehausen (1986). Here, solitary wave speed increases with $\sqrt{A+h}$ rate for waves with larger amplitude. The increase in the solitary wave propagation speed can be observed in Fig. 17, when comparing the wave recorded in Gauge I of Fig. 17(a) with Fig. 17(d), for

example. The peak of the larger wave passes the fixed wave gauges at a faster rate and hence it looks more concentrated.

As the wave amplitude increases, shown in Fig. 17, the effect of the plate on wave is more remarkable, and this is expected. The transmitted wave, although recovers to a soliton shape, has a smaller wave amplitude due to the energy attenuation and transfer beneath the plate. Amplitude of the main reflected soliton, however, does not appear to vary significantly with the incident wave amplitude. In all cases, the solitary wave amplitude above the plate is dropped slightly, and this is due to the energy reflection upwave, and energy transmission below the plate. It is, however, expected that for long plates, the solitary wave amplitude above the plate increases after the initial drop due to smaller water depth.

Time series of solitary wave transformation propagating over plates with different lengths are shown in Fig. 18. The most significant impact of the plate length on the solitary wave transformation is seen at Gauge V, above the plate. As the plate length increases, the second hump has more time to develop and separates from the main soliton, before it arrives at the trailing edge of the plate. Shown in Fig. 18(d), the case of the longest plate, a second hump is about to separate from the original wave. The transmitted wave, however, seems to be independent of the plate length, and it recovers its form, to a large extent, in all cases. Overall, the plate length appears to have little effect on the scattering of the solitary wave.

Time series of solitary wave scattering by plates submerged at different depths are shown in Fig. 19. In Fig. 19(a), $d/h = 0.2$, when the plate is closest to the SWL, it has the most significant impact on wave scattering. In this case, the wave above the plate undergoes significant deformation and faster than other cases, and the transmitted wave has the smallest amplitude. In all cases, the transmitted wave downwave has recovered its original form. The amplitude of the reflected wave, recorded by Gauge II, increases when plate is closer to the SWL.

For a solitary wave, we define the reflection and transmission coefficient by $C_R = \frac{A_R}{A_I}$, $C_T = \frac{A_T}{A_I}$, respectively, where A_I is the incident solitary wave amplitude, and A_R is the amplitude of the main hump reflected from the plate, and A_T is the amplitude of the transmitted soliton. It is observed that the main reflected soliton does not change its form as it propagates away from the leading edge of the plate. The transmitted soliton, however, initially shows some changes immediately downwave of the plate. It then recovers a constant form and keeps its shape as it propagates downwave over the flat seafloor. The amplitude of the transmitted soliton is recorded at a gauge five L_p downwave where the soliton has reached its permanent shape.

The variation of the solitary wave reflection and transmission coefficients with wave amplitude, plate length and the submergence depth are shown in Fig. 20. The wave condition and plate characteristics are same as those discussed in Figs. 17, 18 and 19. The default values of $A/h = 0.2$, $d/h = 0.4$, and $L_p/h = 2$ are selected, and in each case, one parameter is varied while the rest are kept constant.

Shown in Fig. 20(a), the reflection coefficient varies slightly with the wave amplitude, *i.e.* the energy reflection percentage from the submerged plate is independent of the wave amplitude. The transmission coefficient, on the other hand, decreases slightly for waves of larger amplitudes. This is mainly due to the stronger soliton fission process for a larger wave, where larger percentage of the energy is attenuated, forming oscillatory tail waves.

Seen in Fig. 20(b), the reflection coefficient shows a slight increase as the plate length enlarges to about $L_p/h \approx 2$. This is because the effective length (wave above the SWL) of the solitary wave is comparable with the plate length in this case. Beyond this point, the reflection coefficient remains constant up to $L_p/h \approx 7$. It then reduces slightly. As the solitary wave approaches the leading edge of the longer plate, some further fluctuations are observed at the leading and trailing edges. This results in a slightly smaller percentage of the wave reflecting back upwave. The transmission coefficient, shown in Fig. 20(b), decreases slightly with the increase of the plate length. As the soliton propagates over the longer plates, there is more time for it to separate into higher number of solitons, and hence a reduction of the amplitude of the main soliton downwave.

Shown in Fig. 20(c), and similar to the case of cnoidal waves, the plate has less effect on the solitary wave scattering when it is submerged at a deeper depth. The reflection coefficient decreases and the transmission coefficient increases with larger submergence depth. The relation, however,

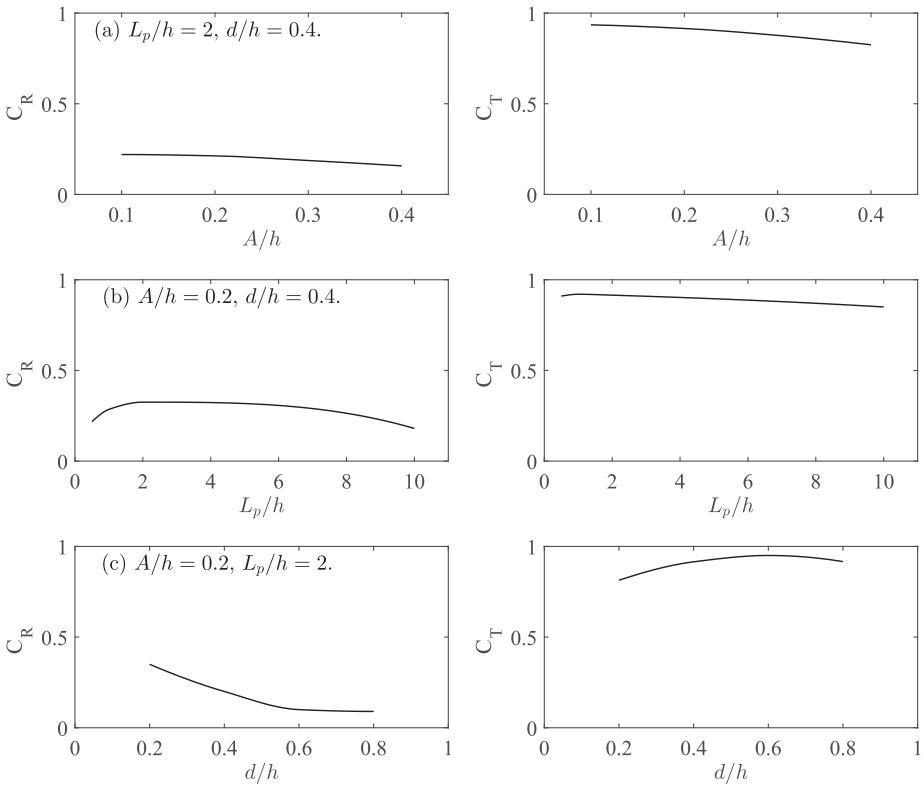

FIG. 20. Variation of solitary wave reflection (C_R) and transmission (C_T) coefficients with (a) wave amplitude (A), (b) plate length (L_P), and (c) submergence depth.

remains nonlinear with slight variation for $d/h > 0.5$, when the plate is submerged at a depth larger than 50% of the water depth.

V. CONCLUDING REMARKS

Nonlinear scattering of cnoidal and solitary waves by a submerged plate is studied by use of the Level I GN equations. When waves encounter a submerged plate, some of the wave energy reflects back due to the fluid-fluid and fluid-structure interactions at the leading edge of the plate. The remaining wave energy transfers above and below the plate mainly, depending on the submergence depth (d/h) and the wavelength over plate length ratio (λ/L_p). Above the plate, waves undergo significant changes due to the sudden reduction in water depth; nonlinearity effects are dominant, wave height increases and waves may ultimately break for large amplitude waves and for $L_p \gg \lambda$. Below the plate, pressure varies linearly between the leading edge and trailing edges, resulting in a uniform and oscillatory flow. Downwave, with the sudden increase of the water depth, dispersion effects are dominant, resulting in the formation of higher nonlinear harmonics and a change in wave frequency, and in principal, a reduction of wave height. The reflection occurs both at the leading edge of the plate, when waves propagate from deep to shallow water, and at the trailing edge, when waves propagate from shallow to deeper depth. The reflection at the leading edge, however, is dominant.

The uniform flow under the plate results in almost instantaneous transfer of energy between the two edges, causing further complication on the wave scattering. At $\lambda/Lp \approx 2.7 - 3.0$, the uniform flow under the plate is at its highest from the trailing edge to the leading edge of the plate. This is approximately the time when the wave crest of the diffracted wave is at the trailing edge of the plate and the trough of the wave is at the leading edge, resulting in maximum wave reflection.

The wave scattering due to a submerged plate is mainly due to the sudden change in the water depth above the plate, and the oscillatory flow beneath the plate. The scattering due to the fluid-fluid interaction is sensitive to the environmental condition that alter the flow field around the submerged

plate, *i.e.* the wavelength to plate length ratio λ/L_p, and the submergence depth of the plate d/h. The close agreement of the GN results with experiments on plates with different thicknesses reveals that the plate thickness does not play any significant role.

For deep and intermediate waves, the wave scattering is characterised by defining the reflection and transformation coefficients. A comparison of the nonlinear wave scattering coefficients of the Level I GN results with the existing laboratory results and other theoretical solutions show an overall good agreement. For highly nonlinear waves, however, higher level GN equations would provide more accurate results. In particular, if energy attenuation and distribution are of interest, high-level GN equations would provide further details about the higher harmonics generated.

For long waves in shallow water, the plate causes a significant energy attenuation by formation of the higher harmonics downwave from the plate. In shallow water and for long waves, the wavelength to plate length ratio does not seem to have a significant role as in deep-water wave condition, but the submergence depth is the dominant factor. The change in wave height, in the case of long waves in shallow water, seems to influence the transmitted wave mostly, with a small impact on the reflected wave. A solitary wave shows a similar behaviour for long waves in shallow water, and this is expected.

The use of a single reflection or transmission coefficient may be appropriate for intermediate to deep water conditions. For nonlinear, shallow-water waves, a significant portion of the energy is allocated to the generation and growth of the higher harmonics, both upwave and downwave from the plate. In shallow water, and for long waves, however, using the reflection and transmission coefficients in describing the energy attenuation may be misleading. The energy distribution due to the generation of higher wave components must also be considered.

A submerged plate may be used as a wave breaker to reduce the severity of the incoming waves. In this case, maximum reflection coefficient and minimum transmission coefficient are desired. It is shown that an optimised wave-plate condition can be obtained for these objectives. The variation of C_R and C_T with the environmental conditions (wave height, wave length and submergence depth), however, is nonlinear. In most cases, it is found that a combination of d/h and λ/L_p defines the optimum condition.

A submerged plate in shallow water can be used as a wave focusing device, resulting in focusing of energy above the plate. The sudden reduction of the water depth results in an increase of the nonlinear effects and a temporary increase of the elevation of the wave crest, followed by the formation of higher harmonics. The wavelength to plate length ratio and the plate submergence depth play a significant role on the wave-focusing phenomenon.

It is shown that in shallow water, the plate has little effect on smaller waves (smaller H/h), and it is mostly influential on waves with larger wave height. Hence, a submerged plate can act as an effective tool for protection of marine aquaculture environments, where some natural wave effects are desired.

Beji, S. and Battjes, J. A., "Numerical simulation of nonlinear wave propagation over a bar," Coastal Engineering **23**(1-2), 1–16 (1994).

Boussinesq, J., "Thorie de l'intumescence liquide appele onde solitaire ou de translation," Comptes Rendus Acad. Sci. Paris **72**, 755–759 (1871).

Brossard, J. and Chagdali, M., "Experimental investigation of the harmonic generation by waves over a submerged plate," Coastal Engineering **42**(4), 277–290 (2001).

Brossard, J., Hemon, A., and Rivoalen, E., "Improved analysis of regular gravity waves and coefficient of reflexion using one or two moving probes," Coastal Engineering **39**(2), 193–212 (2000).

Brossard, J., Perret, G., Blonce, L., and Diedhiou, A., "Higher harmonics induced by a submerged horizontal plate and a submerged rectangular step in a wave flume," Coastal Engineering **56**(1), 11–22 (2009).

Burke, J. E., "Scattering of surface waves on an infinitely deep fluid," Journal of Mathematical Physics **5**(6), 805–819 (1964).

Cao, Y., Schultz, W. W., and Beck, R. F., "Three-dimensional desingularized boundary integral methods for potential problems," International Journal for Numerical Methods in Fluids **12**(8), 785–803 (1991).

Carter, R. W. and Ertekin, R. C., "Focusing of wave-induced flow through a submerged disk with a tubular opening," Applied Ocean Research **47**, 110–124 (2014).

Carter, R. W., Ertekin, R. C., and Lin, P. (2006), On the reverse flow beneath a submerged plate due to wave action, In 25th International Conference on Offshore Mechanics and Arctic Engineering (OMAE), Hamburg, Germany, ASME, pages 595–602.

Cho, I. H., Koh, H. J., Kim, J. R., and Kim, M. H., "Wave scattering by dual submerged horizontal porous plates," Ocean Engineering **73**, 149–158 (2013).

Dattatri, J., Shankar, N. J., and Raman, H. (1977), Laboratory investigations of submerged platform breakwaters, In Proceedings of the 17th Congress of the IAHR, Baden-Baden, W. Germany **4**, pages 89–96.

Demirbilek, Z. and Webster, W. C. (1992), Application of the Green-Naghdi theory of fluid sheets to shallow water wave problems, Technical report, US Army Corps of Engineers, Vicksburg, Mississippi, 48 p.

Demirbilek, Z. and Webster, W. C. (1999), The Green-Naghdi theory of fluid sheets for shallow-water waves, In *Developments in Offshore Engineering: Wave Phenomena and Offshore Topics*, Edt. Herbich, J. B., chapter 1, pages 1–54, Gulf Publishing Company, Houston, Texas, USA.

Dias, F. and Vanden-Broeck, J. M., "Open channel flows with submerged obstructions," Journal of Fluid Mechanics **206**, 155–170 (1989).

Dias, F. and Vanden-Broeck, J. M., "Trapped waves between submerged obstacles," Journal of Fluid Mechanics **509**, 93–102 (2004).

Dick, T. M. and Brebner, A., Solid and permeable submerged breakwaters, In Proceedings of 11th Coastal Engineering Conference, London, ASCE, pages 1141–1158. (1968).

Duffett, J., Beck, R. F., Zhang, X., Maki, K. J., and Newman, J. N. (2016), Experimental and numerical study of waves amplified by a submerged plate, In Proceedings of the 31st Int. Workshop on Water Waves and Floating Bodies (IWWWFB), 3-6 April, Plymouth, MI, USA, pages 37–40.

Ertekin, R. C. (1984), Soliton generation by moving disturbances in shallow water: Theory, computation and experiment, PhD thesis, University of California at Berkeley, May, v+352 pp.

Ertekin, R. C. and Becker, J. M., "Nonlinear diffraction of waves by a submerged shelf in shallow water," Journal of Offshore Mechanics and Arctic Engineering, ASME **120**, 212–220 (1998).

Ertekin, R. C. and Hayatdavoodi, M. (2015), Hydrodynamics of wave forces on Coastal-Bridge decks: Calculations by Euler's equations versus nonlinear shallow-water wave equations, In Proc. Oceans 2015 Conference, MTS/IEEE, Genova, Italy, May 18-21, Paper #141204-084.

Ertekin, R. C., Hayatdavoodi, M., and Kim, J. W., "On some solitary and cnoidal wave diffraction solutions of the Green-Naghdi equations," Applied Ocean Research **47**, 125–137 (2014).

Ertekin, R. C. and Rodenbusch, G. (2016), Wave, current and wind loads, In *Springer Handbook of Ocean Engineering*, Edts. Dhanak, M. R. and Xiros, N. I., pages 787–818, Springer International Publishing.

Ertekin, R. C. and Wehausen, J. V. (1986), Some soliton calculations, In Proc. 16th Symp. on Naval Hydrodynamics, Berkeley, pages 167–185, July, pp. 167-184, Disc, p. 185 (Ed. by W.C.Webster, National Academy Press, Washington, D.C., 1987).

Evans, D. V. and Linton, C. M., "Trapped modes in open channels," Journal of Fluid Mechanics **225**, 153–175 (1991).

Farina, L., "Water wave radiation by a heaving submerged horizontal disk very near the free surface," Physics of Fluids **22**(5), 057102 (2010).

Farina, L. and Martin, P. A., "Scattering of water waves by a submerged disc using a hypersingular integral equation," Applied Ocean Research **20**(3), 121–134 (1998).

Gobbi, M. F. and Kirby, J. T., "Wave evolution over submerged sills: Tests of a high-order Boussinesq model," Coastal Engineering **37**(1), 57–96 (1999).

Gobbi, M. F., Kirby, J. T., and Wei, G. E., "A fully nonlinear Boussinesq model for surface waves. Part 2. Extension to $O(kh)^4$," Journal of Fluid Mechanics **405**, 181–210 (2000).

Goda, Y. and Suzuki, T. (1976), Estimation of incident and reflected waves in random wave experiments, Coastal Engineering Proceedings, Honolulu, Hawaii, **1**(15).

Graw, K. (1993), Shore protection and electricity by submerged plate wave energy converter, In Proceedings of the European wave energy symposium, Edinburgh, Scotland, pages 379–384.

Green, A. E., Laws, N., and Naghdi, P. M., "On the theory of water waves," Proceedings of the Royal Society of London A: Mathematical, Physical and Engineering Sciences **338**(1612), 43–55 (1974).

Green, A. E. and Naghdi, P. M., "A derivation of equations for wave propagation in water of variable depth," Journal of Fluid Mechanics **78**, 237–246 (1976a).

Green, A. E. and Naghdi, P. M., "Directed fluid sheets," Proc. of the Royal Society of London. Series A, Mathematical and Physical Sciences **347**(1651), 447–473 (1976b).

Greene, T. R. and Heins, A. E., "Water waves over a channel of infinite depth," Quarterly of Applied Mathematics **11**(2), 201–214 (1953).

Grue, J., "Nonlinear water waves at a submerged obstacle or bottom topography," Journal of Fluid Mechanics **244**, 455–476 (1992).

Hassan, M.-U., Meylan, M. H., and Peter, M. A., "Water-wave scattering by submerged elastic plates," The Quarterly Journal of Mechanics and Applied Mathematics **62**(3), 321–344 (2009).

Hayatdavoodi, M. (2013), Nonlinear wave loads on decks of coastal structures, PhD thesis, University of Hawaii at Manoa, xiv+186 p.

Hayatdavoodi, M. and Ertekin, R. C., "Nonlinear wave loads on a submerged deck by the Green-Naghdi equations," Journal of Offshore Mechanics and Arctic Engineering **137**(1), 011102-1–011102-9 (2015a).

Hayatdavoodi, M. and Ertekin, R. C., "Wave forces on a submerged horizontal plate. Part I: Theory and modelling," Journal of Fluids and Structures **54**(April), 566–579 (2015b).

Hayatdavoodi, M. and Ertekin, R. C., "Wave forces on a submerged horizontal plate. Part II: Solitary and cnoidal waves," Journal of Fluids and Structures **54**(April), 580–596 (2015c).

Hayatdavoodi, M. and Ertekin, R. C., "Review of wave loads on coastal bridge decks," Applied Mechanics Reviews **68**(3), 030802-1–030802-16 (2016).

Hayatdavoodi, M. and Ertekin, R. C. (2017), Hydroelastic response of a submerged plate to long waves, In 32nd International Workshop On Water Waves And Floating Bodies (IWWWFB32), Dalian, China, 23-26 April, pages 85–88.

Hayatdavoodi, M., Ertekin, R. C., and Thies, J. T. (2017), Conceptual design and analysis of a submerged wave energy device in shallow water, In 36th Int. Conf. on Ocean, Offshore and Arctic Engineering, OMAE '17, ASME, June 25–30, Trondheim, Norway, OMAE2017-62174.

Hayatdavoodi, M., Seiffert, B., and Ertekin, R. C., "Experiments and computations of Solitary-Wave forces on a coastal-bridge deck. Part II: Deck with girders," Coastal Engineering **88**(June), 210–228 (2014).
Hayatdavoodi, M., Seiffert, B., and Ertekin, R. C., "Experiments and calculations of cnoidal wave loads on a flat plate in shallow-water," Journal of Ocean Engineering and Marine Energy **1**(1), 77–99 (2015).
Hayatdavoodi, M., Wagner, J. J., Wagner, J. R., and Ertekin, R. C. (2016), Vertical oscillation of a horizontal submerged plate, In Proceedings of the 31st Int. Workshop on Water Waves and Floating Bodies (IWWWFB), 3-6 April, Plymouth, MI, USA, pages 53–56.
Heins, A. E., "Water waves over a channel of finite depth with a dock," American Journal of Mathematics **70**(4), 730–748 (1948).
Hsu, H. H. and Wu, Y. C., "Scattering of water wave by a submerged horizontal plate and a submerged permeable breakwater," Ocean Engineering **26**(4), 325–341 (1998).
Huang, C. J. and Dong, C. M., "Wave deformation and vortex generation in water waves propagating over a submerged dike," Coastal Engineering **37**(2), 123–148 (1999).
Kim, J. W. and Bai, K. J., "A new complementary mild-slope equation," Journal of fluid Mechanics **511**, 25–40 (2004).
Kim, J. W., Bai, K. J., Ertekin, R. C., and Webster, W. C., " A derivation of the Green-Naghdi equations for irrotational flows," Journal of Engineering Mathematics **40**, 17–42 (2001).
Kim, J. W., Bai, K. J., Ertekin, R. C., and Webster, W. C., "A strongly-nonlinear model for water waves in water of variable depth – the Irrotational Green-Naghdi model," Journal of Offshore Mechanics and Arctic Engineering **125**(1), 25–32 (2003).
Kim, J. W. and Ertekin, R. C., "A numerical study of nonlinear wave interaction in irregular seas: Irrotational Green-Naghdi model," Marine Structures **13**, 331–348 (2000).
Kojima, H., Yoshida, A., and Nakamura, T. (1994). Linear and nonlinear wave forces exerted on a submerged horizontal plate. Proceedings of 24th Conference on Coastal Engineering, Kobe, Japan, pages 1312–1326.
Korteweg, D. J. and De Vries, G., "On the change of form of long waves advancing in a rectangular channel, and a new type of long stationary wave," Philosophical Magazine **39**, 422–443 (1895).
Kuznetsov, N., Maz'ya, V., and Vainberg, B. (2002). *Linear water waves: a mathematical approach*. Cambridge University Press, Cambridge, United Kingdom, p. 532.
Lalli, F., Bruschi, A., Liberti, L., Mandrone, S., Pesarino, V., and Bassanini, P., "Numerical analysis of flat plate breakwater," Coastal Engineering 3668–3680 (2008).
Lin, H. X., Ning, D., Zou, Q. P., Teng, B., and Chen, L. F., "Current effects on nonlinear wave scattering by a submerged plate," Journal of Waterway, Port, Coastal, and Ocean Engineering **140**(5), 04014016 (2014).
Linton, C. M. and Evans, D. V., "Trapped modes above a submerged horizontal plate," The Quarterly Journal of Mechanics and Applied Mathematics **44**(3), 487–506 (1991).
Liu, C., Huang, Z., and Keat Tan, S., "Nonlinear scattering of non-breaking waves by a submerged horizontal plate: Experiments and simulations," Ocean Engineering **36**(17), 1332–1345 (2009).
Liu, P. L.-F., "Diffraction of solitary waves," Journal of Waterway, Port, Coastal, and Ocean Engineering **110**(2), 201–214 (1984).
Liu, P. L.-F. and Abbaspour, M., "Wave scattering by a rigid thin barrier," Journal of the Waterway, Port, Coastal and Ocean Division **108**(4), 479–491 (1982).
Liu, P. L.-F. and Iskandarani, M., "Scattering of short-wave groups by submerged horizontal plate," Journal of Waterway, Port, Coastal, and Ocean Engineering **117**(3), 235–246 (1991).
Lo, H. Y. and Liu, P. L.-F., "Solitary waves incident on a submerged horizontal plate," Journal of Waterway Port Coastal and Ocean Engineering **140**(May/June), 04014009-1–04014009-17 (2014).
Madsen, P. A. and Schäffer, H. A., "Higher–order Boussinesq–type equations for surface gravity waves: Derivation and analysis," Philosophical Transactions of the Royal Society of London A: Mathematical, Physical and Engineering Sciences **356**(1749), 3123–3181 (1998).
Mansard, E. P. D. and Funke, E. R. (1980). The measurement of incident and reflected spectra using a least squares method. Proceedings of 17th Conference on Coastal Engineering, Sydney, Australia, **1**(17).
Martin, P. A. and Farina, L., "Radiation of water waves by a heaving submerged horizontal disc," Journal of Fluid Mechanics **337**, 365–379 (1997).
McIver, M., "Diffraction of water waves by a moored, horizontal, flat plate," Journal of Engineering Mathematics **19**(4), 297–319 (1985).
McIver, M. and Porter, R., "Trapping of waves by a submerged elliptical torus," Journal of Fluid Mechanics **456**, 277–293 (2002).
McIver, P. and Evans, D. V., "The trapping of surface waves above a submerged, horizontal cylinder," Journal of Fluid Mechanics **151**, 243–255 (1985).
Neelamani, S. and Reddy, M. S., "Wave transmission and reflection characteristics of a rigid surface and submerged horizontal plate," Ocean Engineering **19**(4), 327–341 (1992).
Newman, J. N., "Propagation of water waves past long two-dimensional obstacles," Journal of Fluid Mech **23**(1), 23–29 (1965).
Newman, J. N. (2015). Amplification of waves by submerged plates. 30th International Workshop on Water Waves and Floating Bodies (IWWWFB), Bristol, UK, pp. 153–156.
Ning, D., Li, Q., Lin, H., and Teng, B., "Numerical investigation of nonlinear wave scattering by a horizontal submerged plate," Procedia Engineering **116**, 237–244 (2015).
Nwogu, O., "Alternative form of Boussinesq equations for nearshore wave propagation," Journal of Waterway, Port, Coastal, and Ocean Engineering **119**(6), 618–638 (1993).
Ohyama, T., Kioka, W., and Tada, A., "Applicability of numerical models to nonlinear dispersive waves," Coastal Engineering **24**(3), 297–313 (1995).

Parsons, N. F. and Martin, P. A., "Scattering of water waves by submerged plates using hypersingular integral equations," Applied Ocean Research **14**(5), 313–321 (1992).
Parsons, N. F. and Martin, P. A., "Trapping of water waves by submerged plates using hypersingular integral equations," Journal of Fluid Mechanics **284**, 359–375 (1995).
Patarapanich, M. (1978). Wave reflection from a fixed horizontal plate. In Proceedings of the International Conference on Water Resources Engineering, Bangkok, Thailand, pages 427–446. Asian Institute of Technology.
Patarapanich, M., "Maximum and zero reflection from submerged plate," Journal of Waterway, Port, Coastal and Ocean Engineering **110**(2), 171–181 (1984).
Patarapanich, M. and Cheong, H. F., "Reflection and transmission characteristics of regular and random waves from a submerged horizontal plate," Coastal Engineering **13**(2), 161–182 (1989).
Pinon, G., Perret, G., Cao, L., Poupardin, A., Brossard, J., and Rivoalen, E., "Vortex kinematics around a submerged plate under water waves. Part II: Numerical computations," European Journal of Mechanics-B/Fluids (2016).
Poupardin, A., Perret, G., Pinon, G., Bourneton, N., Rivoalen, E., and Brossard, J., "Vortex kinematic around a submerged plate under water waves. Part I: Experimental analysis," European Journal of Mechanics-B/Fluids **34**, 47–55 (2012).
Sampath, R., Montanari, N., Akinci, N., Prescott, S., and Smith, C., "Large-scale solitary wave simulation with implicit incompressible SPH," Journal of Ocean Engineering and Marine Energy **2**(3), 313–329 (2016).
Seiffert, B., Hayatdavoodi, M., and Ertekin, R. C., "Experiments and computations of solitary-wave forces on a coastal-bridge deck. Part I: Flat plate," Coastal Engineering **88**(June), 194–209 (2014)..
Shields, J. J. and Webster, W. C., "On direct methods in water-wave theory," Journal of Fluid Mechanics **197**, 171–199 (1988).
Siew, P. F. and Hurley, D. G., "Long surface waves incident on a submerged horizontal plate," Journal of Fluid Mechanics **83**, 141–151 (1977).
Stamnes, J. J., Løvhaugen, O., Spjelkavik, B., Mei, C. C., Lo, E., and Yue, D. K., "Nonlinear focusing of surface waves by a lens–theory and experiment," Journal of Fluid Mechanics **135**, 71–94 (1983).
Stoker, J. J. (1958). *Water waves: The mathematical theory with applications*. Wiley-Interscience, USA, p. 567.
Stokes, G. G., "Report on recent researches in hydrodynamics," British Association for Advancement of Science **1**, 1–20 (1846).
Sun, X. (1991). Some theoretical and numerical studies on two-dimensional cnoidal-wave-diffraction problems. Master's thesis, Department of Ocean Engineering, University of Hawaii at Manoa, Honolulu, xii+149 pp.
Ursell, F., "Trapping modes in the theory of surface waves," Mathematical Proceedings of the Cambridge Philosophical Society **47**(2), 347–358 (1951).
Ursell, F., "Mathematical aspects of trapping modes in the theory of surface waves," Journal of Fluid Mechanics **183**, 421–437 (1987).
Usha, R. and Gayathri, T., "Wave motion over a twin-plate breakwater," Ocean Engineering **32**(8), 1054–1072 (2005).
Utsunomiya, T. and Eatock Taylor, R., "Trapped modes around a row of circular cylinders in a channel," Journal of Fluid Mechanics **386**, 259–279 (1999).
Webster, W. C. and Shields, J. J. (1991). Applications of high-level Green-Naghdi theory to fluid flow problems. In Proceedings of Symposium on Dynamics Marine Vehicles and Stuctures in Waves, Elsevier, Uxbridge, U.K., pages 109–124.
Webster, W. C. and Wehausen, J. V. (1995). *Bragg scattering of water waves by Green-Naghdi theory*, pages 566–583. Birkhäuser Basel, Basel.
Wei, G., Kirby, J. T., Grilli, S. T., Subramanya, R. *et al.*, "A fully nonlinear Boussinesq model for surface waves. Part 1. Highly nonlinear unsteady waves," Journal of Fluid Mechanics **294**(7), 71–92 (1995).
Wei, Z. and Dalrymple, R. A., "Numerical study on mitigating tsunami force on bridges by an SPH model," Journal of Ocean Engineering and Marine Energy, 1–16 (2016).
Williams, T. D. and Meylan, M. H., "The Wiener–Hopf and residue calculus solutions for a submerged semi-infinite elastic plate," Journal of Engineering Mathematics **75**(1), 81–106 (2012).
Wu, D. and Wu, T. Y. (1982). Three-dimensional nonlinear long waves due to moving surface pressure. In Proceedings of the 14th Symposium on Naval Hydrodynamics, Washington, D.C., pages 103–125. National Academy Press, Washington, D.C.
Wu, T., "Long waves in ocean and coastal waters," Journal of Engineering Mechanics Division, ASCE **107**(3), 501–522 (1981).
Yu, X. and Chwang, A. T., "Analysis of wave scattering by submerged circular disk," Journal of Engineering Mechanics **119**(9), 1804–1817 (1993).
Yu, X. and Chwang, A. T., "Water waves above submerged porous plate," Journal of Engineering Mechanics **120**(6), 1270–1282 (1994).
Zhang, S. and Williams, A. N., "Wave scattering by submerged elliptical disk," Journal of Waterway, Port, Coastal, and Ocean Engineering **122**(1), 38–45 (1996).
Zhao, B. B., Duan, W. Y., and Ertekin, R. C., "Application of higher-level GN theory to some wave transformation problems," Coastal Engineering **83**, 177–189 (2014a)..
Zhao, B. B., Duan, W. Y., Ertekin, R. C., and Hayatdavoodi, M., "High-level Green–Naghdi wave models for nonlinear wave transformation in three dimensions," Journal of Ocean Engineering and Marine Energy **1**(2), 121–132 (2015).
Zhao, B. B., Ertekin, R. C., Duan, W. Y., and Hayatdavoodi, M., "On the steady solitary-wave solution of the Green-Naghdi equations of different levels," Wave Motion **51**(8), 1382–1395 (2014b).